34487

NAME OF AUTHOR / *NOM DE L'AUTEUR*___ Brian Jeffrey STACKHOUSE

TITLE OF THESIS / *TITRE DE LA THÈSE*___ SINGLE CRYSTAL ELECTRICAL RESISTIVITIES

IN CADMIUM AND CADMIUM—MAGNESIUM ALLOYS.

UNIVERSITY / *UNIVERSITÉ*___ UNIVERSITY OF ALBERTA

DEGREE FOR WHICH THESIS WAS PRESENTED /
GRADE POUR LEQUEL CETTE THÈSE FUT PRÉSENTÉE___ Ph. D.

YEAR THIS DEGREE CONFERRED / *ANNÉE D'OBTENTION DE CE GRADE*___ 1977

NAME OF SUPERVISOR / *NOM DU DIRECTEUR DE THÈSE*___ DR. S. B WOODS

DATED / *DATE*___ Sept. 20, 1977 ___ SIGNED / *SIGNÉ*___ Brian Stackhouse

PERMANENT ADDRESS / *RÉSIDENCE FIXÉ*___ 71 ANDERS CLOSE,

RED DEER, ALBERTA

T4R 1C2

THE UNIVERSITY OF ALBERTA

SINGLE CRYSTAL ELECTRICAL RESISTIVITIES

OF CADMIUM AND CADMIUM-MAGNESIUM ALLOYS

by

Ⓒ   BRIAN JEFFREY STACKHOUSE

A THESIS

SUBMITTED TO THE FACULTY OF GRADUATE STUDIES AND RESEARCH

IN PARTIAL FULFILLMENT OF THE REQUIREMENTS FOR THE DEGREE

OF DOCTOR OF PHILOSOPHY

IN

PHYSICS

DEPARTMENT OF PHYSICS

EDMONTON, ALBERTA

FALL, 1977

THE UNIVERSITY OF ALBERTA

FACULTY OF GRADUATE STUDIES AND RESEARCH

The undersigned certify that they have read,
and recommend to the Faculty of Graduate Studies and
Research, for acceptance, a thesis entitled SINGLE
CRYSTAL ELECTRICAL RESISTIVITIES OF CADMIUM AND
CADMIUM-MAGNESIUM ALLOYS submitted by Brian Jeffrey
Stackhouse in partial fulfillment of the requirements
for the degree of Doctor of Philosophy in Physics.

....
Supervisor

....

....

....

....
External Examiner

Date 9 September 1977

ABSTRACT

We have measured the electrical resistivities from 2 K to 300 K for eight Cd single crystals and twelve Cd-Mg single crystals including three different concentrations. The measured densities of our specimens were typically 2½% below the accepted x-ray densities. This we attribute to small bubbles in the specimens and we have made an appropriate correction to obtain the resistivity values. The ice point resistivities for Cd were found to be $\rho_{||}$ = 7.81($\pm$0.03)$\mu\Omega$ cm and $\rho_{\perp}$ = 6.30($\pm$0.03)$\mu\Omega$ cm. The resistivity anisotropy ratio $a = \rho_{||}/\rho_{\perp}$ was obtained for both Cd and the most dilute alloy at all temperatures and compared to theoretical models.

Deviations from Matthiessen's rule Δ which were also calculated from these measurements both confirm and clarify earlier experimental results for polycrystalline specimens and agree qualitatively with a theoretical calculation for single crystals. A contribution to Δ appearing above $\sim$ 200 K has all the salient features expected for electron scattering from a local phonon mode. Although Damon and Klemens predicted and sought for such an effect, it has not previously been recognized.

We emphasize that errors in geometrical shape factors ℓ/A for our specimens and in the correction for bubbles do not significantly affect the temperature (T) variation of

a or Δ and in particular the qualitative features of the Δ-T curve which we associate with the local mode.

ACKNOWLEDGEMENTS

Finally, I thank my wife Donna for her patience,

assuming many of my family responsibilities over the past

five years while I've been elsewhere.

TABLE OF CONTENTS

Page

LIST OF TABLES

x

LIST OF FIGURES

CHAPTER 1

INTRODUCTION

Seth and Woods (1970) measured deviations from
Matthiessen's Rule (DMR or Δ) in a series of complementary
dilute binary alloys (metal A in metal B and B in A) to test
the theory of Bhatia and Gupta (1969) about the effect of an
interference term on DMR at high temperatures. For tempera-
tures (T) above about 120 K, DMR were found to be linear in
T, as expected, for all alloys except Cd-Mg, and, also as
expected, negative for one alloy of each complementary pair,
again except for the Cd-Mg pair. The high temperature slopes
of the Δ versus T curves were negative for both Mg-Cd alloys
(Hedgcock and Muir, 1964; Das and Gerritsen, 1964) and Cd-Mg
alloys (Seth and Woods, 1970). In addition, the Δ-T curves
for the Cd-Mg alloys were only linear from at it 80 K to
220 K where the slopes of these curves began to increase to
more positive values. Seth and Woods suggest their apparently
anomalous results could be due to different textures – grain
structures and degrees of preferred crystallite orientation –
in different specimens. In a review on DMR, Bass (1972)
suggests looking in anisotropic metals for anisotropy in Δ.
Toussaint and Pecheur (1973) have in fact calculated curves
for Δ-T in Cd-Mg and Mg-Cd for single crystal orientations
both parallel and perpendicular to the c axis. Their calcul-
ations result in negative values of $d\Delta_3/dT$ for both Cd-Mg and
Mg-Cd at high temperatures, and furthermore, predict that Δ_3

the contribution to Δ due to the interference term, differs
in the two symmetry directions by an order of magnitude.
Measurements of DMR on single crystals would surely clarify
the situation.

A second topic of recent interest is the temperature
dependence of the anisotropy ratio, $a = \rho_{||}/\rho_{\perp}$. Case and
Gueths (1970) measured the anisotropy ratio in tin and
found a striking maximum of $a_{max.} = a_{\infty}^2$ (where a_{∞} is the
extrapolated value of a as $T \to \infty$) at about 20 K. Completely
neglecting any effects due to anisotropy in the phonon
spectrum, they explain their results in terms of a simpli-
fied model of the Fermi surface and predict the same temp-
erature behaviour for any electrically anisotropic metal.
In a review on galvanomagnetic effects in anisotropic metals,
Hurd (1974) points to an urgent need for comparable data
on other metals to test Case and Gueth's simple model. A
number of more thorough calculations, including one by
White and Carbotte (1974) on Zn (which has a similar c/a
ratio and Fer $\perp$ s rface to Cd) have provided theoretical
alternatives to Case and Geuths for comparison with
experiment.

With both of the above problems in mind, we have pre-
pared long, thin single crystals of varying crystal orienta-
tions, eight of high purity cadmium metal and twelve of
dilute $\underline{Cd}$-Mg alloys with three different concentrations.
Electrical resistivities, the anisotropy ratio $a = \rho_{||}/\rho_{\perp}$

and deviations from Matthiessen's Rule have been measured as functions of temperature from about 2 K to 330 K.

The next four chapters include respectively a brief outline of the theoretical background for these problems (Chapter 2), a description of our experimental procedure including specimen preparation (Chapter 3), the presentation of our experimental data and explanation of various corrections which have been made to the data (Chapter 4) and a discussion of our results (Chapter 5). The final chapter (Chapter 6) is a brief summary of our conclusions. At the end of the thesis are the bibliography and four appendices of which Appendix 1 on notation will be of most frequent use to the reader.

CHAPTER 2

THEORETICAL BACKGROUND

2.1 Ideal Resistivity and Anisotropy Ratio in Hexagonal Metals

An electric field, $\vec{E}$, produces an electric current density, $\vec{J}$, according to

$$J_i = \sigma_{ij} E_j \qquad i,j = 1,2,3 \qquad (2.1)$$

where σ_{ij} is the electrical conductivity tensor. For metals with cubic crystal structures, $\vec{J}$ is always parallel to $\vec{E}$ and the tensor reduces to a constant. For metals with hexagonal crystal structures, the conductivity tensor has two independent components as shown:

$$\begin{pmatrix} J_1 \\ J_2 \\ J_3 \end{pmatrix} = \begin{pmatrix} \sigma_\perp & 0 & 0 \\ 0 & \sigma_\perp & 0 \\ 0 & 0 & \sigma_{||} \end{pmatrix} \begin{pmatrix} E_1 \\ E_2 \\ E_3 \end{pmatrix} \qquad (2.2)$$

J_3 and E_3 are the components of $\vec{J}$ and $\vec{E}$ parallel to the c axis, the axis of six-fold or hexagonal symmetry. $\sigma_\perp$ and $\sigma_{||}$ are the electrical conductivities perpendicular to and parallel to the c axis. $\rho_\perp = 1/\sigma_\perp$ and $\rho_{||} = 1/\sigma_{||}$ are the analogous components of the electrical resistivity tensor $\rho_{ij} = (\sigma_{ij})^{-1}$.

In long thin cylindrical single crystals of orientation θ (see Appendix 1 for notation), the resistivity $\rho(\theta)$ is the component of $\vec{E}$ parallel to $\vec{J}$ (which is parallel to the specimen axis) divided by $|\vec{J}|$ or:

$$\rho(\theta) = \vec{E}\cdot\vec{J}/|\vec{J}|^2 \qquad (2.3)$$

It can easily be shown that:

$$\rho(\theta) = \rho_{||}\cos^2\theta + \rho_{\perp}\sin^2\theta \qquad (2.4)$$

Note that resistivity is also a function of temperature and specimen composition, as well as orientation. For simplicity in notation throughout this thesis, the explicit dependence on one or more of these variables is often omitted.

Note secondly that there is also a component of $\vec{E}$ perpendicular (or transverse) to $\vec{J}$ for $0° < \theta < 90°$. We show in Appendix 2 how both $\rho_{\perp}$ and $\rho_{||}$ can be obtained by measuring the parallel and the perpendicular components of $\vec{E}$ in one single crystal.

In general, $\rho_{||} \neq \rho_{\perp}$ and the anisotropy ratio is defined as $a = \rho_{||}/\rho_{\perp}$, a function of both temperature and specimen composition.

Theoretical calculations of electrical resistivity generally start with the Boltzmann transport equation

(Ziman, 1969). $f = f_{\vec{k}}$ is the electron distribution function, the probability that an electron state with wave vector $\vec{k}$ will be occupied. Under the influence of an electric field, the distribution function will change until a steady state is reached where

$$\left(\frac{\partial f}{\partial t}\right)_{\text{field}} + \left(\frac{\partial f}{\partial t}\right)_{\text{scatt.}} = 0 \qquad (2.5)$$

$\left(\frac{\partial f}{\partial t}\right)_{\text{field}}$ and $\left(\frac{\partial f}{\partial t}\right)_{\text{scatt.}}$ are the rates at which the distribution function is changed by the electric field and by scattering processes respectively.

The electric current density, $\vec{J}$, is found by integrating the distribution function multiplied by the electron velocity, $\vec{v}_{\vec{k}}$, times the electron charge, e, over all possible $\vec{k}$ states according to:

$$\vec{J} = 2 \int e \, \vec{v}_{\vec{k}} \, f_{\vec{k}} \, d^3\vec{k}. \qquad (2.6)$$

Since $f_{\vec{k}}$ depends on $\vec{E}$, Eq. 2.6 is analogous to Eq. 2.1 and the conductivity tensor can be found by solving Eq. 2.5 and Eq. 2.6. In practice, this is difficult to do and simplifying assumptions are made.

Anisotropy in the electrical conductivity (and thus resistivity) arises because of:

(1) anisotropy of the Fermi surface

(2) anisotropy of the scattering process,

including anisotropy of the phonon spectrum (Pecheur and Toussaint, 1972). Since the scattering process is strongly dependent on temperature, the resistivity anisotropy $a = \rho_{||}/\rho_{\perp}$, is also expected to be temperature dependent.

Case and Gueths (1970) proposed a simple theory for a_T based on an anisotropic Fermi surface beyond the first Brillouin zone but completely neglected the effects of anisotropy in the phonon spectrum. Their model predicts for any anisotropic metal, a maximum $a_{max} = a_{\infty}^2$ at low temperatures ($\sim$ 20 K for Sn) falling off as $(a_T - a_{\infty}) \propto T^{-2}$ at high temperatures, a_{∞} being the anisotropy as T $\rightarrow \infty$. They further predict that $a_{\infty} = \rho_{||\infty}/\rho_{\perp\infty} = A_{\perp}/A_{||}$ where $A_{||}$ and $A_{\perp}$ are the areas of the Fermi surface extending beyond the Brillouin zone boundaries in the c ($||$) and a ($\perp$) directions respectively. A final consequence of their theory is that a_0, the anisotropy ratio as T $\rightarrow$ 0, should return to the high temperature limit of a_{∞}. In spite of their oversimplified model, their own experimental results of the resistivity anisotropy for Sn show remarkable agreement with their predictions.

A number of other theorists, particularly Pecheur and Toussaint as well as Carbotte and co-workers have proposed more extensive calculations of electrical resistivities, initially for isotropic metals but more recently, these calculations have been extended to anisotropic materials as well. Most useful for comparison with the

experimental results presented in this thesis are the

calculations by White and Carbotte (1974). They have

found an approximate solution to the Boltzmann equation

using a relaxation time approximation where the calculated

relaxation times vary over the Fermi surface and take into

account the phonon dispersion curves measured by inelastic

neutron scattering. They plot curves of a versus tempera-

ture for pure Zn and also for dilute alloys of Zn, the

latter both with and without the residual resistivities

subtracted from the total resistivities. Qualitatively,

the curve for pure Zn has all of the features predicted by

Case and Gueths, except that a drops markedly below a_∞

at the lowest temperatures. Unfortunately, Cd strongly

absorbs neutrons so that it is not possible to similarly

obtain the phonon spectrum for Cd. However, the c/a ratios

for Cd and Zn are similar as are their Fermi surfaces, so

a comparison of our experimental results with their pre-

dictions is not unreasonable even without taking account

of the different phonon spectra.

2.2 Deviations from Matthiessen's Rule

For a   ce binary alloy, the total resistivity

ρ_{AT} may be wr   as

$$\rho_{AT} = \rho_{A} \quad \tau + \Delta_T \tag{2.7}$$

where ρ_{Ao} is the residual resistivity extrapolated as

$T \rightarrow 0$, ρ_{1T} is the "ideal" resistivity for the pure host metal, and Δ_T is the "deviation from Matthiessen's rule" (DMR). For oriented single crystals of uniform impurity concentration; ρ_{AT}, ρ_{Ao} and ρ_{1T} are all linear in $\cos^2\theta$ according to Eq. 2.4. Consequently, $\Delta_T(\theta)$ is also linear in $\cos^2\theta$ for a given concentration and can be written

$$\Delta_T(\theta) = \rho_{AT}(\theta) - \rho_{Ao}(\theta) - \rho_{1T}(\theta) \qquad (2.8a)$$

$$\Delta_T(\theta) = \Delta_{||T} \cos^2\theta + \Delta_{\perp T} \sin^2\theta \qquad (2.8b)$$

The explicit dependence of $\Delta_T(\theta)$ on concentration is omitted for simplicity.

Almost by definition, Δ_T is small with respect to ρ_{AT}. Since resistivities have not been calculated exactly, one would expect even less precision in theoretical calculations of DMR. Indeed, since about 1947, many theories for DMR have appeared, several of them still controversial. Bass (1972) has reviewed the subject and assessed the success of various theoretical models in the light of experimental work.

The features of DMR which have been reported in experiments on several metals include:

- (1)   a strong temperature dependence at lowest temperature, of the form T^n where n varies from about 3 to 5.

(2) a hump in many alloys at intermediate tempera-
tures, often near the temperature where $\rho_{Ao} \simeq \rho_{1T}$.

(3) a linear region at relatively high temperatures
(T ≳ 150 K for many alloys) of the form $\Delta = mT + b$ where

m and b are constants, b > 0 and m may be either positive
or negative.

A fourth feature expected in some alloy systems due
to a localized phonon mode (Damon and Klemens, 1965) is a
change in slope to a more positive value at high tempera-
tures ($\sim$ 200 K for Cd-Mg). In previous experiments this
feature had not been recognized.

A number of mechanisms have been proposed to give
rise to DMR. Although Bass (1972) gives a more complete
list, the most important ones are:

(1) Inelastic electron-impurity scattering - For
Matthiessen's rule to be valid, electrons are assumed to be
scattered inelastically by phonons and elastically by
static impurities, both processes operating independently.
Because the impurities are not static, electrons can also
be scattered inelastically by vibrating impurities.
Koshino (1960) calculated that a DMR proportional to T^2 at
low temperatures would arise from one-phonon inelastic
scattering by impurities. Taylor (1962, 1964) showed that
two-phonon processes could not be neglected in the calcu-
lations and although he ultimately predicted a T^2 dependence
as well, the term would be too small to measure. Klemens

(1963) produced a T^4 ... ... of DMR case

on a time varying strain field around the impurities.

The T^4 variation is in qualitative agreement with experiment (Damon, Mathur and Klemens, 1968) for $T \lesssim 20$ K.

(2) Two-band model - Initially proposed by Sondheimer and Wilson (1947), the two-band model assumes that relaxation times are not isotropic on the Fermi surface (e.g. neck and belly regions in noble metals) and the anisotropies are different for two kinds of scattering mechanisms (i.e. impurities and phonons). Even though Matthiessen's rule is assumed to hold in each individual region, the two regions or bands, acting like resistors in parallel (i.e. their conductivities add), produce a DMR which is proportional to ρ_{iT} at low temperatures (where $\rho_{iT} \ll \rho_{Ao}$) and proportional to ρ_{Ao} at high temperatures. In a modification of the two-band model where the ratio of the ideal resistivities in the two bands is not constant, but a monotonic function of temperature, Dugdale and Basinski (1967) show that a hump which would be sharpest for the most dilute alloys could be produced at a temperature where $\rho_{iT} \sim \rho_{Ao}$.

(3) Interference Term - Kagan and Zhernov (1966) and Bhatia and Gupta (1969) calculated a contribution to the DMR from interference between scattering by impurities and scattering by phonons. Although values estimated by Kagan and Zhernov were too low to explain experimental

results, the term given by Bhatia and Gupta below was of the correct order of magnitude.

$$\Delta_3 = D\ 2c \int_0^1 W_A\ (W_B-W_A)\ S_{av}(x)x^3\ dx \qquad (2.9)$$

where $D = 12\pi m^2/\hbar^3 e^2 k_F^2$, $x = q/2k_F$, W_A and W_B are pseudo-potential matrix elements for atom types A and B in a binary A-B alloy, and c (in this equation only*) is the fraction of B atoms. Δ_3 is significant at high temperatures where it is linear and may be either positive or negative (whereas all previous theories predicted strictly positive contributions to Δ in this temperature region). Furthermore, the sign of Δ_3 would largely depend on the sign of $W_A(W_B-W_A)$ in the neighbourhood of $x = 1$ and one would often expect the sign of Δ_3 to be opposite for complementary alloys (A-B and B-A). Toussaint and Pecheur (1973) have calculated values of Δ_3 for single crystals of Cd-Mg and Mg-Cd in parallel and perpendicular orientations. For both systems, they find negative values of Δ_3 which are an order of magnitude larger for the parallel orientation than for the perpendicular orientation and they suggest experiments on single crystals as a possible check of the importance of the interference term. Unfortunately, it appears that in their calculations they have employed only the pure

*Elsewhere in this thesis, x refers to atomic fraction of atoms (i.e. concentration) and c is the lattice parameter perpendicular to the hexagonal planes.

metal pseudopotential matrix elements, W_{Cd} and W_{Mg}, which may very well be significantly different from the pseudo-potential matrix elements for the dilute alloys.

(4) Anisotropy of the electron distribution function — Kagan and Zhernov (1971) were able to explain the observed variation of DMR over the entire temperature range in terms of anisotropy of the nonequilibrium electron distribution function. In the pure metal, this anisotropy arises primarily because of umklapp processes and may cause a decrease in the ideal resistivity of orders of magnitude. As impurities are added to the metal, elastic scattering by the impurities tends to suppress the anisotropy of the distribution function and the resistivity approaches the value expected for an isotropic distribution function.

(5) Local modes — When a dilute binary alloy consists of light impurity atoms in a lattice of heavier atoms, local modes of high frequency, ω_o, appear in the phonon spectrum above the continuum (Damon and Klemens, 1965). Assuming that the interatomic force constants are the same for all atoms including the impurities,

$$\omega_o \simeq (M_1/M_o)^{\frac{1}{2}} \omega_D \qquad (2.10)$$

where M_1 and M_o are the masses of the host and impurity atoms respectively and ω_D is the Debye frequency for the pure metal. Scattering by these localized phonon modes

would produce an increase in the electrical resistivity starting at about $\frac{1}{2}\Theta_o$ where $\Theta_o = \hbar\omega_o/k_B$ is the characteristic temperature of the local mode ($\hbar$ is Planck's constant divided by 2π and k_B is Boltzmann's constant). This appears as a contribution to DMR, Δ_4, where

$$\Delta_4 \propto \Theta_o/(\exp(\Theta_o/T)-1). \qquad (2.11)$$

On a Δ-T graph, Δ_4 is expected to produce a change of slope to a more positive value at about $T = \frac{1}{2}\Theta_o$ (~ 200 K for Cd-Mg).

The interest in the experiments described in this thesis centers around the contributions to DMR, Δ_3 due to the interference term and Δ_4 due to local modes.

CHAPTER 3

EXPERIMENTAL DETAILS

Seth (1969) outlines the experimental procedures necessary for measuring deviations from Mattiessen's rule (DMR or Δ_T) and these procedures are more than adequate for measuring resistivity anisotropy. In order to calculate Δ_T with reasonable accuracy, the geometrical shape factor $f = l/A$ (where l is the length between potential contacts on a specimen of cross-sectional area A), the resistances R_T at all temperatures, and the residual resistances R_0 extrapolated as $T \rightarrow 0$ K must all be measured extremely accurately. Specimens, up to ten at a time, must be held at the same constant temperature during each measurement, whereas only modest accuracy is necessary in determining the temperature itself.

Aside from the specimen preparation, many of the experimental details are similar to Seth's work but with a number of improvements, most notably the specimen holder and the current comparator. Over the course of these experiments, further improvements suggested themselves but often too late to be incorporated. Some of these are summarized in Appendix 3 on suggestions for future resistivity measurements.

3.1 The Cryostat and Temperature Control

The cryostat and specimen holder used for the   -

15

Pumping Tubes
Needle Valve
Vapour Pressure Line

Pumping Chamber

Thermal Anchoring Post for Leads
Post for mounting Specimen Holder

Outer Can
Shield
Inner Can

Thermometers

Specimen

Brass Rods (1/8" dia)
Brass Collar
'Tufnol' Disc

Specimen Holder

Potential Contact to Specimen
Current Contact between Specimens
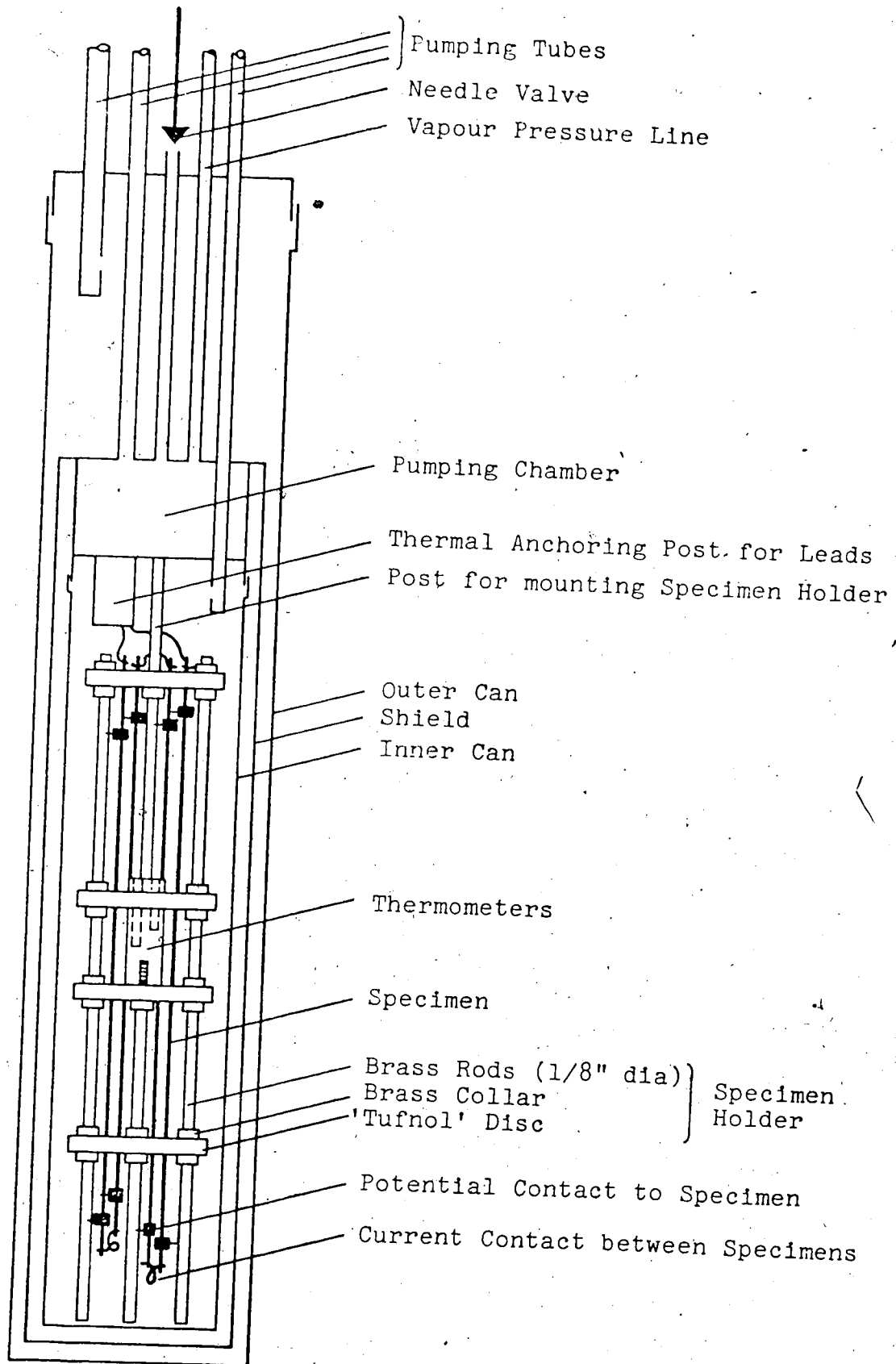
Fig. 1   Cryostat and Specimen Holder

resistance measurements are shown in Fig. 1. In order
to free enough electrical leads to measure ten specimens
simultaneously, the measuring current was brought into
the cryostat through leads but returned through the
stainless steel pumping tube. Aside from this modifica-
tion, the cryostat is as Seth (1969) described.

The specimen holder consists of four 'Tufnol' discs,
2 in. in diameter and 1/4 in. thick, spaced 1 - 3 in.
apart and held rigidly on three 1/8 in. diameter brass
rods, 9 1/4 in. long by movable brass collars with et
screws. The specimens, typically 8 in. long and 1 mm in
diameter, slid freely through a series of aligned holes
in the 'Tufnol' discs. The specimens were connected in
series by soldering them at the ends to thin copper wires
(AWG #28) and were supported in the specimen holder by the
soldered current connection at the top end of each speci-
men. Each wire was tinned with Sn-Pb solder (60% Sn)
and had a double loop allowing both specimens and wires to
expand and contract freely. Soldered current connections
were used because local Joule heating at mechanical con-
tacts can be significant, particularly at low temperatures.
The resistance between potential contacts on adjacent
specimens was measured at 4.2K to check roughly that the
solder joint resistances were low. Low resistance solder
joints were most difficult to make on the alloy specimens
of highest magnesium content. Care was taken during the

soldering process not to damage the single crystals beyond the immediate region of the solder joint.

To avoid constraining the specimens during thermal expansion or contraction, potential contacts were attached to the specimens only and not to the specimen holder. Thus, in addition to its own weight ($\sim$ 1.5 g), each specimen supported two potential contacts ($\sim$ 0.2 g each) consisting of a small 'Tufnol' cylinder 7 mm long and 5 mm in diameter with a hole slightly larger than the specimen diameter drilled perpendicular to the cylinder axis. A small pointed brass screw parallel to the cylinder axis held the cylinder in place and made electrical contact with the specimen. The contacts should not be screwed any further than necessary into the specimen because the size of the indentation determines the uncertainty in length ℓ, typically 1 part in 2000, a significant source of error in the ultimate values for resistivity. Finally, an electrical lead was soldered to the other end of the brass screw, the entire procedure executed with great care to avoid straining the single crystal specimens.

Resistances were measured at 4.2 K with a refrigerant bath of liquid He^4 at atmospheric pressure around the outer can. Temperatures below 4.2 K were obtained by pumping above liquid He^4 in the pumping chamber while maintaining a vacuum of better than 10^{-5} Torr in the outer can. A resistance bridge temperature controller was used

to obtain constant temperatures between 4.2 K and 63 K. To control the temperature, the amplified signal due to the difference between resistances of a carbon resistor mounted on top of the pumping chamber and a variable resistance set at a desired value, modulated the power fed to a 100Ω 1 watt heating resistor also mounted on top of the pumping chamber. Because the resistance of the carbon resistor was a strongly varying function of temperature, this controller provided a sensitive means of attaining stable temperatures, particularly below 77 K.

Liquid nitrogen was used as the refrigerant bath to obtain thermal equilibrium at 77 K and temperatures down to 63 K could be obtained by pumping above liquid nitrogen. From 77 K to about 260 K, stable temperatures were obtained using both the resistance bridge temperature controller and an additional 8 watt 1200Ω resistor fed by a variac. Additional measurements were made at room temperature, at 273.2 K using an ice water bath and, for the last run only, at 314 K and 327 K using warm water baths.

Thermal drift first became noticeable at about 15 K. From that temperature upwards, the sequence of readings consisted of measuring temperature, measuring the specimen resistances, remeasuring the temperature, remeasuring the specimen resistances, and finally measuring the temperature a third time. This procedure took about thirty minutes (or longer at the lowest temperatures where

readings were taken to the limits of the voltage sensi-
tivity) and during that time the drift in temperature was
typically ±0.02 K above 77 K and ±0.003 K below 77 K.
The temperature drift was roughly linear in time so that
by interpolating between the two sets of resistance
measurements, it was possible to estimate the resistances
at the time the second temperature was measured to about
2 parts in 10^5 except where voltage sensitivity was the
limiting factor. Although by waiting longer, one could
have attained a more stable temperature before measuring
the specimens, this was both impractical from the point of
view of time and unnecessary for accuracy.

3.2 Temperature Measurement

A platinum resistance thermometer was used to
measure temperatures above 77 K. This thermometer had been
calibrated against another platinum resistance thermometer
which the National Research Council of Canada had cali-
brated. The calibration points of resistance versus
temperature were fitted to a Callendar-Van Dusen equation
in order to determine intermediate temperatures. The
resistance was measured by passing the same electric
current of about 100μA through both the thermometer and a
Leeds and Northrup 1000Ω standard resistor, and measuring
the potential differences across each with a Fluke Model
8800A Digital Multimeter.

Below 77 K, temperature was measured with a germanium resistance thermometer which had been calibrated against an N.B.S. germanium thermometer from 2 K to 12 K and an N.R.C. platinum thermometer above 12 K. Temperatures for resistances between the calibration points were determined by graphical interpolation from 2 K to 12 K and by a computer least squares fit to an eleventh degree polynomial above 12 K. The resistance of the germanium thermometer was measured by a D.C. resistance comparator (Seth, 1969) using a Guildline 9801T precision four-terminal variable resistor for the comparison.

Both thermometers were inserted in wells in a copper cylinder, 1½ in. long and 1/2 in. in diameter, supported in the middle of the array of specimens by two of the 'Tufnol' discs in the specimen holder. The thermometers were coated with Wakefield thermal compound to improve the thermal contact with the copper cylinder.

Temperatures were determined to an accuracy of about ±0.025 K. Temperature stability however was an order of magnitude better i.e. the temperature at which the specimen resistances were measured was the same for all specimens to within a few milliKelvin (mK).

3.3 Resistance Measurement

A Guildline Model 9920 Direct-Current Comparator Bridge was used to compare the currents through an unknown

resistance (a specimen) and a four terminal standard
resistor when the potential differences across each were
balanced. The ratio of the unknown resistance to the
standard resistance R_s could then be read directly to 1
part in 10^7 of R_s from seven dials on the comparator.

The difference in potentials could be zeroed with a
sensitivity of about 1nV using a Guildline Type 5214/9460
Photocell Galvanometer Amplifier and a Guildline Type
9461-A Galvanometer. A constant specimen current of
$\sim$ 100 mA meant specimen resistances could be determined
to $\sim$ $10^{-8}\Omega$.

Above 77 K, the standard resistor was a calibrated
Guildline four-terminal 1Ω 0.1 watt standard resistor with
a temperature coefficient of -1 ppm/°C. A four-terminal
0.01Ω standard resistor was used below 77 K. This
resistor was calibrated against the 1Ω standard resistor
and found to be independent of current up to 1A to better
than 1 part in 10^5. For room temperatures between 22½°C
and 28½°C, the 0.01Ω resistor had constant resistance to
better than 1 part in 10^4. The two standard resistors
were compared twice each run by measuring the specimens
at 77 K against both.

Typical specimen resistances were 0.02Ω at 295 K
and ranged at the lowest temperatures from 0.000002Ω for
the pure specimens to 0.001Ω for some of the alloys.
Nanovolt sensitivity was utilized at low temperatures for

all specimens while the comparator's seven figure accuracy was necessary only for the alloy specimens at low temperatures where $\rho_{Ao} \gg \rho_{iT}$ and $d\rho_{AT}/dT$ was small.

3.4   Specimen Preparation

The cadmium used in all specimens was obtained from Consolidated Mining and Smelting Co. of Canada and had 59 grade purity. The magnesium used in the dilute Cd-Mg alloy specimens was obtained from Johnson, Matthey and Co. and had impurities of less than 14 ppm.

3.4:1   Pure Cadmium Specimens

Long, thin cadmium single crystals of random orientations were grown using a Bridgman technique (Bridgman, 1925).

Cadmium ingots were placed in the funnel shaped top of a Pyrex mold after both the ingots and glassware had been rinsed with dilute hydrochloric acid, distilled water and isopropyl alcohol in succession and dried quickly by blowing helium gas over them. A loose fitting lid covered the mold to reduce evaporation losses of the cadmium. The mold itself was thin walled Pyrex tubing of approximately 1 mm inside diameter and about 25 cm long, closed to a point at the bottom.

Thin walled Pyrex tubing was readily available and could be dissolved relatively quickly (in about 2 hours)

using small quantities of hydrofluoric acid. The small variations in cross-sectional area, A, typically ±1% along a 20 cm specimen, do not produce a significant error in $f = \ell/A$ when an average value of A is determined by weighing a known specimen length and using known density values.

A vertical furnace was lowered over part of a vacuum system in which the Pyrex mold was supported. T furnace consisted of a 20 in. length of 2 in. diameter st in ss steel tubing around which were wrapped a layer of asbestos paper for electrical insulation, a 'Kanthal' ribbon heating element and several additional layers of asbestos paper for thermal insulation. The top of the furnace was filled with glass wool to reduce convective heat losses.

The resistance of the winding was about 40Ω and a 0-140V variac connected to the mains supplied the power. The furnace had been wound to obtain a steep thermal gradient at the bottom of the mold and a gradual thermal gradient towards the top. A variac setting of 120V brought the bottom of the mold to approximately the melting point of cadmium (321°C), the upper part of the mold being hotter.

A vacuum of about 10^{-4} Torr was maintained for several hours while the cadmium ingots in the funnel at the top of the mold were gradually heated to near the melting point. The variac was then turned up to 140V and the

ingots melted in about ten minutes. This was done quickly
to minimize evaporation losses of the molten metal.
Helium gas was admitted to the section of the vacuum
system inside the furnace, forcing the molten cadmium
down into the 1 mm diameter tubing. The variac was lower-
ed to 120V and the system approached thermal equilibrium
at that setting with a time constant of about 30 minutes.
After about an hour, a small motor was turned on. It
raised the furnace at a uniform rate of $\sim$ 4 cm/hour until
the furnace was completely above the specimen.

The Pyrex mold was dissolved in concentrated hydro-
fluoric acid and the specimen was rinsed with dilute
hydrochloric acid, distilled water and isopropyl alcohol
in succession and then dried. Each specimen was x-rayed
at four points along its length both before and after
being measured in a run. Orientations were determined to
$\sim$ $\pm 1°$ by analyzing the Laue back reflection patterns.
Nearly all of the specimens grown in this way turned out
to be single crystals and with a few exceptions, the
crystal orientations were constant within $\pm 1°$ along each
specimen's length. The good variety of specimen orienta-
tions obtained this way, including the most desirable
orientations close to parallel and close to perpendicular,
meant that growing specimens from seed crystals was not
necessary.

Although the resistance ratios R_{295}/R_o were typically

$\sim 10^4$ for the pure cadmium specimens, there was some evidence of strain in the single crystals. Some of the Laue back reflection patterns were blurred, particularly when looking along crystal directions perpendicular to the c axis in which case the spots were often smeared out in the direction towards the c axis. Secondly, the residual resistances of Cd #24 and Cd #25, the two specimens used in all three reported runs, decreased by about 4-5% in the three month period during which these runs were made. These specimens had been grown about one month prior to the first of these runs and except during the runs themselves (of about a week to ten days each), the specimens were stored at room temperature.

Several possible specimens had been annealed for 12 hours at 125°C in an attempt to reduce strain. Indeed, the x-ray patterns did appear sharper after annealing and residual resistances were reduced. Unfortunately though, this procedure resulted in some recrystallization, observed both visually as well as with x-rays, and some of the best specimens were ruined. None of these annealed specimens are included in the experiments reported here.

With the exception of one specimen (which had been grown four years earlier and which is also not included in the results presented here), there was no visual or x-ray evidence that any of the specimens measured in the three runs had recrystalliz at all.

3.4.2 Cd-Mg Alloy Specimens

Three master alloys of cadmium with approximately
0.76, 1.5, and 5.6 atomic percent magnesium were made.
For each master alloy, the cadmium and magnesium ingots
were rinsed with dilute hydrochloric acid, distilled
water, and isopropyl alcohol and then dried. The ingots
were weighed and put into a Pyrex container consisting
of thin walled tubing about 30 cm long and ∿ 6 mm inside
diameter with a bulb of ∿ 4 cm diameter on one end. The
container was evacuated, then refilled with partial
pressures of about 10 Torr of hydrogen gas (to prevent
oxidation of the magnesium) and about half an atmosphere
of helium gas, and then sealed. Using the same furnace
described in Sec. 3.4.1 (as it could be easily removed
from the motorized raising apparatus), the ingots in the
bulb were heated to above the melting point of cadmium.
The magnesium was initially observed floating in the
molten cadmium. The whole furnace was shaken vigourously
for 15 seconds every three minutes and after about twenty
minutes no solid magnesium could be seen in the molten
alloy. To ensure complete solution and thorough homo-
genization, the above shaking procedure was continued
for a further twenty minutes. Then, the entire furnace
was inverted, allowing the molten alloy to run quickly
into the long, sealed tubing which protruded out of the
furnace section. The alloy solidified within two minutes,

forming crystallites with dimensions of $\sim$ 1 mm or less.
After cooling, the Pyrex tubing was dissolved in hydro-
fluoric acid and the master alloy rinsed with dilute
hydrochloric acid, distilled water and isopropyl alcohol
and then dried.

To check that each master alloy was homogeneous,
four potential contacts (similar to those described in
Sec. 3.1 but proportionately larger) were attached along
the length of the master alloy splitting it into three
sections and the resistances of each section were
measured at room temperature and at 4.2 K. For each
master alloy, the values of $R_{295}/R_{4.2}$ were the same to
within 0.5% for all three sections (except for one section
of the Cd1.5Mg master alloy which was 4% lower than the
other two sections and which was not used to make speci-
mens), indicating uniform magnesium concentration along
the length of each master alloy.

Side cutters were used to cut off sections 1 to 2 cm
long from the master alloy. These sections were rinsed
and dried and used to grow crystals in the same way
described for the pure cadmium specimens (Sec. 3.4.1).
The only difference was that the alloy specimens were
raised to the melting point under a pressure of about
5 Torr of hydrogen gas, to prevent oxidation of the
magnesium, whereas the pure cadmium had been melted under
vacuum.

3.4.3 Specimen Analysis

Because of possible preferred evaporation and/or inhomogeneities in the specimens, the magnesium concentrations in the alloy specimens should be checked against some independent standard. The most reliable yardstick for this measurement was the set of residual resistivities for Seth's (1969) polycrystalline $\underline{Cd}$-Mg specimens. These are summarized in Table 1.

According to Nordheim's rule (Meaden, 1965), the residual resistivity ρ_o of a binary alloy is proportional to $x(1-x)$ or $\sim x$ for a dilute alloy where x is the atomic fraction of the solute i.e. the concentration. Indeed, Seth's ρ_o's for $\underline{Cd}$-Mg do agree well with Nordheim's rule. Because ρ_{295} does not depend strongly on concentration, the resistivity ratio ρ_o/ρ_{295} is also nearly linear in x so that specimen concentrations can be determined by interpolating values of the resistance ratios $R_o/R_{295} \approx \rho_o/\rho_{295}$ and are thus independent of the ℓ/A determination (which itself depends on the density of the alloy, the density in turn depending on the concentration).

For single crystals, the resistivities, ρ_o and ρ_{295}, and thus the resistance ratios R_o/R_{295} also depend on orientation according to Eq. 2.4. Since the four single crystals grown from the Cd0.76Mg master alloy do show the expected variation with $\cos^2\theta$ (see Sec. 5.2 including Figs. 5 and 6), this series of alloys was used

Table 1

ρ_0, ρ_{295}, and ρ_0/ρ_{295} as functions of magnesium concentration in cadmium for polycrystalline wires (from Seth, 1969)

Mg conc. (at. %)	ρ_0 ($\mu\Omega$ cm)	ρ_{295} ($\mu\Omega$ cm)	ρ_0/ρ_{295}
0.0	0.0020	7.6090	0.00026
0.75	0.2217	7.7519	0.02861
1.5	0.4960	8.0462	0.06167
3.0	0.9920	8.4221	0.11738

to determine the orientation dependence of the resistance ratio.

To compa: the resistivities of polycrystalline specimens and single crystals, Meaden (1965) uses

$$\rho_{poly} = (1/3)\rho_{||} + (2/3)\rho_{\perp} \qquad (3.1)$$

The resistivity of a polycrystalline specimen ρ_{poly} is the same as that of a single crystal with an orientation such that $\cos^2\theta = 1/3$. We assume with this formula that there is no preferred orientation in the polycrystalline specimen. Although Seth's specimens do appear to have preferred orientations slightly closer to parallel than expected (see Sec. 5.2), this will not produce a significant error in the final results.

The magnesium concentrations determined by comparing the resistance ratios R_o/R_{295} to the ratios for Seth's specimens and allowing for the orientation dependence of the ratios are listed in Table 2. Also included in Table 2 are the specimen densities and the specimen bubble factors (see Sec. 3.5 and Sec. 4.1.3). The densities which are based on lattice parameters given by Pearson (1958) and which assume atomic masses of 112.41 and 24.305 for Cd and Mg respectively, depend on the Mg concentration. The calculated bubble factors depend in

Table 2

Magnesium concentration (atomic percent), densities (g/cm^3) and bubble factors at 295 K for Cd-Mg alloy specimens.

Specimen	Mg Concentration	Density	Bubble Factor
Pure Cd	0.00	8.645	0.021-0.032
Cd0.76 Mg Master Alloy	0.90(±.04)[†]		
Cd0.76Mg #3	0.78(±.04)	8.596(±.005)	0.028
Cd0.76Mg #5	0.78(±.04)	8.596(±.005)	0.030
Cd0.76Mg #6	0.78(±.04)	8.596(±.005)	0.022
Cd0.76Mg #8	0.78(±.04)	8.596(±.005)	0.029
Cd1.5Mg Master Alloy	1.73(±.08)[†]		
Cd1.5Mg #1	1.34(±.08)	8.560(±.008)	0.033
Cd1.5Mg #2	1.23(±.07)	8.567(±.007)	0.031
Cd1.5Mg #3	1.42(±.15)	8.555(±.012)	0.032
Cd1.5Mg #4	1.40(±.11)	8.556(±.009)	0.029
Cd5.6Mg Master Alloy	5.0(±.5)[†]		
Cd5.6Mg #2*	1.63(±.11)	8.542(±.009)	0.076
Cd5.6Mg #3*	1.66(±.11)	8.540(±.009)	0.089
Cd5.6Mg #4*	1.89(±.14)	8.525(±.011)	0.069
Cd5.6Mg #5*	1.80(±.12)	8.531(±.010)	0.077

*These calculations assume the alloys are homogeneous which is not the case for the Cd5.6Mg specimens.

†Master alloy concentrations were determined using $R_{4.2}/R_{295}$ rather than R_o/R_{295}.

turn on the calculated densities.

For the Cd0.76Mg and Cd1.5Mg specimens, the calcu-
lated concentrations are reasonably close to the expected
concentrations based on the weights of the Cd and Mg
ingots before alloying (i.e. 0.76 at. % and 1.5 at. %).
The calculated concentrations for the Cd5.6Mg specimens,
however, are significantly lower than expected, even
though the Cd5.6Mg master alloy had close to the expected
concentration. The calculated bubble factors which depend
on the density and concentration calculations are also
anomalously large for the Cd5.6Mg alloys.

To look for small scale specimen homogeneity, an
x-ray microanalysis with an electron probe was performed*
on one specimen for each magnesium concentration. Whereas
the Cd0.76Mg and Cd1.5Mg specimens did appear reasonably
homogeneous on this scale, the Cd5.6Mg specimen was
definitely not homogeneous. Although the results obtained
using this technique cannot be used to determine accurate
absolute Mg concentrations, they indicated that the
Cd5.6Mg specimen did contain significantly more Mg than
the other two specimens. These results suggest that
during the growth of the single crystals much of the
magnesium went into some more ordered state (a Cd_3Mg

superlattice is a possibility) than a random substitution-
al alloy (this type of explanation would also account
largely for the high calculated bubble factors), but the
phase diagram for Cd-Mg given by Hansen (1958) doesn't
show any other phase close to that magnesium concentration.
Because of the inhomogeneity in this specimen and the
absence of a good explanation for it, the Cd5.6Mg speci-
mens are omitted from the results presented in this thesis.

3.5 Experimental Procedure

The average cross-sectional area of each specimen
was determined by weighing a known length of the specimen
and using assumed densities based on lattice parameters
(Pearson, 1958). Average cross-sectional areas were also
calculated from diameter measurements using a micrometer
caliper and found to be typically 2½% larger for both
specimen diameters of $\sim$ 1 mm and $\sim$ 3 mm.

Assuming that the discrepancy in cross-sectional
area is due to voids throughout the bulk of the specimen,
a travelling potential probe (Seth, 1967) was used to
scan the specimen for large voids which did not appear
on the surface. By measuring the resistance of 10 cm
lengths at $\sim$ 1 cm intervals along the specimen, a large
void would appear as an increase or decrease in the
resistance as the probe moved along the specimen to
include or exclude a void in the 10 cm length. Because

of the uncertainty in the length, this probe could only 'see' voids with dimensions of $\sim$ 1/2 the specimen diameter ($\sim$ 1/4 of the specimen cross section) or larger. No voids which were not already apparent visually on the surface were detected.

Specimens selected for measurement were mounted in the specimen holder with the potential contacts positioned on the specimens to exclude any large voids, and the inner can was soldered on. The inner can was then immersed in liquid nitrogen to ensure that a good vacuum could be obtained and then warmed to room temperature so the outer can could be soldered on. Although this procedure effectively constituted thermal cycling no systematic change in the resistance of the specimens was observed, probably because the specimens were able to expand and contract freely in the specimen holder.

After the run, the specimens were removed and the length, ℓ, between the indentations made by the potential contacts was measured by a cathetometer with the telescope replaced by a microscope. The specimen was cut with a razor blade as close to the indentation points as possible. This length, ℓ' ($\sim \ell$), was weighed and the average cross-sectional area was remeasured as previously described. The geometrical shape factor, $f = \ell/A$ was calculated from these measurements.

CHAPTER 4

EXPERIMENTAL RESULTS

4.1 Analysis of Results

Electrical resistivities were calculated from the measured resistances and the measured geometrical shape factors at 293 K $f_{293} = (\ell/A)_{293}$ according to

$$\rho_T = R_T (A/\ell)_T \qquad (4.1)$$

where $(A/\ell)_T$ has been corrected for thermal expansion as described in Sec. 4.1.1. Although it would also be appropriate to correct experimental resistivities for changes in atomic volume (Sec. 4.1.2), this correction cannot be calculated with confidence and has therefore not been applied. In Sec. 4.1.3, a correction to Eq. 4.1 due to bubbles in the specimens is explained. Sources of error, primarily in the geometrical shape factor $f = \ell/A$ are discussed in Sec. 4.1.4. Finally, in Sec. 4.1.5 the experimental results with calculated values of resistivities, the anisotropy ratio $\alpha = \rho_{||}/\rho_{\perp}$ and deviations from Matthiessen's rule Δ are presented in tables. Graphical presentation of the data is included in Chapter 5 where the results are discussed.

4.1.1 Corrections for Thermal Expansion

Thermal expansion affects the electrical resistivities
of anisotropic single crystals in three ways:

(1) because thermal expansion is anisotropic, the
crystal experiences slight changes in orientation with
changes in temperature.

(2) the geometrical shape factor changes with
temperature and because thermal expansion is anisotropic,
the correction for this change depends on specimen orienta-
tion.

(3) the atomic volume changes on thermal contraction,
an effect discussed in Sec. 4.1.2.

McCammon and White (1965) gave a table of linear
expansion coefficients for cadmium in directions both
parallel to and perpendicular to the c axis from 293 K to
3 K. From their data, values of $(L_T/L_{293})_{||}$ and
$(L_T/L_{293})_\perp$ have been calculated and are tabulated in
Table 3.

Because of anisotropic thermal contraction, the
orientation θ_T at a temperature T differs slightly from
the orientation θ_{293} measured at 293 K. In Appendix 4,
it is shown that

$$\tan \theta_T = \frac{(L_T/L_{293})_\perp}{(L_T/L_{293})_{||}} \tan \theta_{293} \qquad (4.2)$$

Table 3

$(L_T/L_{293})_{||}$, $(L_T/_{293})_\perp$ and correction factors for thermal contraction $(f_{||293}/f_{||T})$ and $f_{\perp293}/f_{\perp T})$ as functions of temperature (K) for pure cadmium.

Temp.	$(L_T/L_{293})_{||}$	$(L_T/L_{293})_\perp$	$(f_{||293}/f_{||T})$	$(f_{\perp293}/f_{\perp T})$
293	1.0000	1.0000	1.00000	1.00000
280	.99929	.99975	1.00021	.99929
260	.99819	.99937	1.00055	.99819
240	.99709	.99900	1.00091	.99709
220	.99598	.99865	1.00133	.c⋯8
200	.99486	.99832	1.00179	.⋯
180	.99374	.99801	1.00230	.99374
160	.99262	.99772	1.00285	.99262
140	.99149	.99745	1.00345	.99149
120	.99034	.99720	1.00411	.99034
100	.98918	.99698	1.00484	.98918
80	.98800	.99679	1.00566	.98800
60	:98680	.99665	1.00660	.98680
40	.98565	.99660	1.00767	.98565
20	.98471	.99665	1.00873	.98471
0	.98451	.99668	1.00900	.98451

This change in orientation is largest for specimen
orientations near 45° and at the lowest temperatures but
even under these conditions, the change is negligible
($\theta_T - \theta_{293} \gtrsim 0.35°$). Even so, this correction has been
applied in plots of ρ versus $\cos^2\theta$ at low temperatures
(Figs. 3 and 6 in Chapter 5).

The corrections to the geometrical shape factors
$f = \ell/A$ which will depend on both temperature and orienta-
tion can also be calculated using the data in Table 3.
For example, the shape factor at temperature T for a
specimen whose axis is parallel to the c axis ($\theta = 0°$)
would be:

$$f_{||T} = \left[\frac{\ell}{A}\right]_{||T} = \frac{\ell_{293} \, (L_T/L_{293})_{||}}{A_{293} \, (L_T/L_{293})_{\perp}^2} \qquad (4.3a)$$

$$= f_{||293} \frac{(L_T/L_{293})_{||}}{(L_T/L_{293})_{\perp}^2}$$

Similarly,

$$f_{\perp T} = f_{\perp 293} \frac{(L_T/L_{293})_{\perp}}{(L_T/L_{293})_{||}(L_T/L_{293})_{\perp}} . \qquad (4.3b)$$

For off-axis orientations:

$$(L_T/L_{293})_{\theta} = (L_T/L_{293})_{||}\cos^2\theta + (L_T/L_{293})_{\perp}\sin^2\theta. \qquad (4.4)$$

This result assumes that the orientation θ is independent

of temperature. In fact, the orientation does change
with temperature, but as previously mentioned the change
is negligible. When the orientation change is included
in Eq. 4.4, the final resistivities change by less than 1
part in 10^4. Using Eq. 4.4, the shape factor at
temperature T is:

$$f_T(\theta) = \left[\frac{(L_T/L_{293})_{||}\cos^2\theta + (L_T/L_{293})_{\perp}\sin^2\theta}{(L_T/L_{293})_{\perp}\{(L_T/L_{293})_{\perp}\cos^2\theta + (L_T/L_{293})_{||}\sin^2\theta\}}\right]$$

$$\times\ f_{293}(\theta). \qquad\qquad (4.5)$$

Since resistivities are calculated by dividing by
f_{293}, these resistivities have been multiplied by a
correction factor $f_{293}(\theta)/f_T(\theta)$, a function of both
orientation and temperature which can be found using
Eq. 4.5. Values of the correction factor for specimens
in the two extreme orientations ($\theta = 0°$ and $\theta = 90°$) are
also included in Table 3. As one can see, the orienta-
tion dependence is significant.

Pearson (1958) gives lattice parameters above 293 K
for Cd and Cd-Mg alloys from which thermal expansion
coefficients can be calculated. By interpolating the
thermal expansion coefficients to dilute alloys (the
alloys Pearson quotes have 9.4, 22.0 and 24.8 at. % Mg),
they appear to be within 5% of the values for pure Cd.

Thermal expansion data for <u>Cd</u>-Mg alloys are not available below 293 K and consequently, the same correction that is applicable to pure Cd also has been used for the alloys.

4.1.2 Corrections due to Changes in Atomic Volume

Theoretical resistivity calculations assume that the atomic volume is constant. Because the atomic volume changes on both thermal contraction and alloying, the electrical resistivities should be corrected for this change. Dugdale and Basinski (1967) calculated a correction which is based on the pressure derivatives of the resistivities.

The strains e_{xx} and e_{zz} in the a and c directions respectively under uniform hydrostatic pressure p can be calculated from the elastic compliance constants s_{ij} according to:

$$
\begin{pmatrix} e_{xx} \\ e_{yy} \\ e_{zz} \\ e_{yz} \\ e_{zx} \\ e_{xy} \end{pmatrix} = \begin{pmatrix} s_{11} & s_{12} & s_{13} & 0 & 0 & 0 \\ s_{12} & s_{11} & s_{13} & 0 & 0 & 0 \\ s_{13} & s_{13} & s_{33} & 0 & 0 & 0 \\ 0 & 0 & 0 & s_{44} & 0 & 0 \\ 0 & 0 & 0 & 0 & s_{44} & 0 \\ 0 & 0 & 0 & 0 & 0 & 2(s_{11}-s_{12}) \end{pmatrix} \begin{pmatrix} p \\ p \\ p \\ 0 \\ 0 \\ 0 \end{pmatrix} \quad (4.6)
$$

Using Bridgman's values quoted by Alexandrov and Ryzhova (1961) for the compliance constants of Cd, we find the

strain in the c direction due to uniform pressure to be nine times the strain in the a direction at room temperature. Changes in length due to the thermal contraction are not nearly as anisotropic, the ratio in thermal expansion coefficients $\alpha_{||}/\alpha_{\perp}$ being about three at room temperature. Because the nature of the volume changes due to uniform hydrostatic pressure and thermal contraction is different in anisotropic metals, any correction which assumes these processes to be equivalent is questionable. Furthermore, precise data on the temperature dependence of $d\rho/dp$ is not available (Seth, 1969). For these reasons, the resistivities quoted here have not been corrected for changes in atomic volume due to thermal contraction.

For similar reasons, no correction has been applied for changes in atomic volume on alloying. Such a correction would also be based on pressure-resistivity data and would depend on correlating two even more different effects - the addition of impurities on localized sites and the application of uniform pressure. Because adding Mg to Cd produces a decrease in c but an increase in a (c and a being the lattice parameters), the effect of pressure on atomic volume does not even agree qualitatively in this respect with alloying. In addition, one must also assume that the thermal expansion of the alloys and the pure metal are the same, until accurate expansion

data for the alloys becomes available below room tempera-
ture. Finally, there is no pressure-resistivity data
available for Cd-Mg alloys.

Dugdale and Basinski (1967) estimate their largest
correction to be about 1/3 of the measured DMR at room
temperature. Although we do agree that corrections would
be appropriate if they could be calculated confidently,
these calculations require too many assumptions and
approximations to justify that confidence. Since Seth
and Woods (1970) have also left out these corrections for
many of the same reasons, our results on DMR in single
crystals can be directly compared with theirs in poly-
crystalline specimens.

4.1.3 Corrections due to Bubbles

The cross-sectional areas of the specimens calcula-
ted from weighings were found to be systematically ∿ 2½%
lower than micrometer measured cross-sections. This
discrepancy represents the 'bubble factor' B, the
fraction of the specimen volume which consists of voids
or bubbles, many of them visible on the surface. The
bubble factors for each specimen have been included in
Tables 2, 4a, 4b, 4c, 5a, and 5b.

To correct the resistivities for the effect of
bubbles, we utilize an equation given by Landauer (1952)
for the electrical conductivity of binary metallic mixtures:

$$\sigma_m = \tfrac{1}{4} \{ (3x_2-1)\sigma_2 + (3x_1-1)\sigma_1$$

$$+ [((3x_2-1)\sigma_2 + (3x_1-1)\sigma_1)^2 + 8\sigma_1\sigma_2]^{\frac{1}{2}} \} \qquad (4.7)$$

where σ_1, σ_2 and σ_m are the electrical conductivites of material 1, material 2 and the mixture, and x_1 and x_2 are the fractions of the total volume occupied by materials 1 and 2 respectively. To obtain this result, Landauer solved Maxwell's equations for spherical inclusions of one material embedded in the uniform mixture. If material 2 represents bubbles, then $\sigma_2 = 0$, $x_2 = B$, $x_1 = 1-B$ and Eq. 4.7 simplifies to:

$$\sigma_m = (1 - 1.5B)\sigma_1 \qquad (4.8)$$

Similarly, in terms of resistivities:

$$\rho_1 = (1 - 1.5B)\rho_m \qquad (4.9)$$

The calculated resistivities based on cross-sectional areas found by weighing specimens is effectively

$$\rho_{1calc} = (A_1/\ell)R$$

$$= ((1-B)A_{total}/\ell)R \qquad (4.10)$$

$$= (1-B)\rho_m$$

where A_1 is the average cross-sectional area of material 1 only found by weighing (thus excluding the cross-sectional area of the bubbles) and A_{total} is the total cross-sectional area measured with the micrometer caliper. Comparing Eqs. 4.9 and 4.10, we see that the calculated resistivities underestimate the effect of bubbles. Resistivities have therefore been multiplied by a correction factor $(1-1.5B)/(1-B)$.

A crude way of interpreting this is to think of each bubble as having two 'shadows', small volumes of material one in front of and one behind the bubble which together have a volume of one half the bubble volume and which do not conduct electricity. Although the weighing procedure eliminates the non-conducting bubbles from the calculation of effective cross-sectional area (Eq. 4.10), it does not eliminate the non-conducting shadows. If the bubbles had been either flattened or elongated the relative volume of the shadows and therefore the necessary correction would have been larger or smaller.

Earlier experimenters have also had problems with

bubbles. Bridgman (1925) discusses the importance of
getting rid of occluded gas before making single crystals.
Unfortunately, molten cadmium evaporates quickly under a
vacuum so that Bridgman's technique of washing the molten
metal back and forth for up to an hour or more is
impractical. This procedure would be particularly in-
convenient for the alloys because of preferential evapora-
tion of one of the two components. Edwards et al (1952)
reported a discrepancy of ∿ 2% between the measured density
and the x-ray density for C̲d̲-Mg alloys (but not for pure
Cd), although Ridley (1964) obtained consistent densities
for ingots whose preparation included swaging to ensure
freedom from porosity.

4.1.4 Accuracy of Results

The major source of error was in determining
accurately the geometrical shape factor $f = \ell/A$ for the
specimens. Using the screw type potential contacts, the
probable error in ℓ/A was about 2 parts in 10^3. The
pointed brass screws were set in far enough to make good
electrical contact (in the case of one specimen,
Cd0.76Mg #6, electrical contact was lost from about 8 K
to 56 K but later regained), thus leaving a finite pit and
corresponding uncertainty. In spite of prior thermal
cycling, the resistivities and deviations from Matthiessen's
rule occasionally showed small discrepancies when several

measurements were taken at approximately the same temperature, usually 77 K or room temperature. As the nature of these discrepancies were not systematic (Cd0.76Mg #5 and Cd0.76Mg #8 show opposite effects at 77 K), possibly the exact point on the specimen at which electrical contact was made varied over the course of a run. Another small error was introduced when the specimens were cut prior to weighing. In addition to the uncertainty in the length measurement, the specimens appeared to stretch slightly during the cutting procedure. The mass of a specimen was typically 1.5 g with an uncertainty of ± 0.5 mg. A final error, applicable only to the alloy specimens, is the uncertainty in density produced by the uncertainty in magnesium concentration. All of these errors are included in the uncertainties in $(\ell/A)_{295}$ which are quoted for each specimen in Tables 4a, 4b, 4c, 5a, and 5b.

An additional error arises when the correction due to bubbles is applied to the resistivities. Because of errors in the micrometer measurement of specimen diameter, the probable error in determining the bubble factor is ± 0.004 and the resulting probable error in the corrected resistivities $\pm 0.2\%$. Although this is effectively another error in ℓ/A, it has been indicated separately in the tables.

4.1.5 Presentation of Data

The data in Tables 4a, 4b, 4c, 5a, and 5b include the measured values of electrical resistance and the electrical resistivites, ρ_i and ρ_A of pure and alloy specimens, as well as calculated values of ideal resistivity anisotropy $a_i = \rho_{||}/\rho_{i\perp}$ and deviations from Matthiessen's rule Δ for each alloy specimen. Both ρ_i and ρ_A have been calculated with the correction for thermal expansion of the geometrical shape factor ($f = \ell/A$) included. Although the correction factor for bubbles $(1-1.5B)/(1-B)$ is not included in the $f = \ell/A$ values quoted in the tables, it has been included in the calculations of the resistivities.

For the pure cadmium specimens, the residual resistivities have been subtracted in determining ρ_i, whereas, the residual resistivities have not been subtracted in determining the alloy resistivities, ρ_A. $\rho_{i||}$ and $\rho_{i\perp}$ were determined at 273.15 K and 26.34 K (where the anisotropy ratio is near its maximum value) by fitting the ideal resistivities of all 8 pure Cd specimens to $\cos^2\theta$ (see Figs. 2 and 3 in Chapter 5). The lines which pass ½% below the point for Cd #24 (θ = 88 3/4°) and ¼% below the point for Cd #25 (θ = 8°) in each graph represent best visual fits for these data. At other temperatures, $\rho_{i||}$ and $\rho_{i\perp}$ were calculated using the resistivities of Cd #24 and Cd #25 only and assuming the

same fit. The anisotropy ratio $a_i = \rho_{i||}/\rho_{i\perp}$ was then calculated.

A special procedure was used for Cd #24 because of a reasonably large bubble in the middle of it. Four potential contacts were attached along its length and the electrical resistance was determined between three different pairs of contacts at each temperature. The section which showed the least variation in resistance with thermal cycling (this type of small discrepancy has been discussed in Sec. 4.1.4) over the course of a run was used in the calculations of $\rho_{i||}$ and $\rho_{i\perp}$.

Deviations from Matthiessen's rule were calculated for each alloy specimen according to:

$$\Delta_T(\theta) = \rho_{AT}(\theta) - \rho_{Ao}(\theta) - \rho_{iT}(\theta) \qquad (2.8a)$$

where θ is the orientation of the alloy specimen and $\rho_{iT}(\theta)$ is determined from the calculated axial resistivities according to

$$\rho_{iT}(\theta) = \rho_{i||T} \cos^2\theta + \rho_{i\perp T} \sin^2\theta \qquad (2.4)$$

Resistances are accurate to about 1 part in 10^4 at high temperatures and about $\pm.005\mu\Omega$ at low temperatures. (Note that for the alloy specimens, this is considerably better than 1 in 10^4) whereas resistivities are only

accurate to ~ 2 in 10^3 because of uncertainties in ℓ/A. Subscripted numerals in the following tables are not significant in absolute magnitude. However, the fourth decimal place in Δ is significant in determining the temperature variation above about 65 K. Also, even though ρ_{AT} and ρ_{Ao} are never themselves significant beyond the fourth decimal point due to the uncertainty in ℓ/A, their difference $\rho_{AT} - \rho_{Ao}$ is significant to ~ 3 in 10^3 and is used to determine Δ. The extra figures are quoted in ρ_{AT} below about 19 K for this reason.

Table 4a

R($\mu\Omega$), ρ_1($\mu\Omega$ cm) and a_1 as functions of Temperature (K) for pure cadmium specimens used in Run #3.

Cd #24 (Bottom) $\quad R_o = 1.410 \ (\pm.005)\mu\Omega$

$\theta = 88 \ 3/4° \ (\pm1\tfrac{1}{4}°)$

$(\ell/A)_{295} = 1388.1(\pm3) \ \text{cm}^{-1}$

$B_a = 0.023(\pm0.004)$

Cd #25 $\quad R_o = 4.241(\pm.005)\mu\Omega$

$\theta = 8° \ (\pm3°)$

$(\ell/A)_{295} = 3454.4(\pm4) \ \text{cm}^{-1}$

$B = 0.026(\pm0.004)$

	Cd #24 (Bottom)		Cd #25		
Temp.	R	ρ_1	R	ρ_1	a_1
2.18	1.42_0	0.00000_7	4.25_3	0.00000_3	—
2.99	1.44_0	0.00002_1	4.29_0	0.00001_4	0.7
4.13	1.56_4	0.00010_8	4.59_0	0.00010_0	0.9
4.20	1.57_6	0.00011	4.56_5	0.00009_3	0.8
6.09	2.69_0	0.00089_7	7.20_0	0.00085_2	0.95
7.73	5.74_0	0.00303_4	15.76_0	0.00331_8	1.10
9.89	14.56_5	0.00921_9	43.57_0	0.01133	1.236
13.16	42.83_0	0.02903	139.46	0.03894	1.352
18.86	136.46	0.09465	477.43	0.1363	1.452

Table 4a (cont'd)

	Cd #24 (Bottom)			Cd #25		
Temp.	R	ρ_1		R	ρ_1	a_1
26.34	322.87	0.2254		1145.13	0.3284	1.470
28.66	389.85	0.2724		1377.10	0.3952	1.464
36.92	651.36	0.4559		2242.06	0.6439	1.424
47.96	1031.5	0.7230		3431.25	0.9855	1.374
62.02	1533.8	1.0764		4948.3	1.421	1.330
76.85	2057.4	1.446		6512.3	1.869	1.302
76.87	2058.1	1.446		6516.3	1.870	1.302
76.88	2058.1	1.446		6516.7_5	1.870	1.303
76.94	2059.9_5	1.447		6522.6	1.872	1.302
77.15	2061.3	1.448		6524.4	1.872	1.302
77.16	2068.1	1.453		6544.7	1.878	1.302
93.67	2651.0	1.865		8285.3	2.377	1.283
124.90	3736.5	2.634		$11543._3$	3.308	1.264
150.54	4621.8	3.263		$14222._3$	4.073	1.256
177.69	5557.3	3.929		$17067._4$	4.884	1.251
197.36	6236.1_5	4.414		$19141._5$	5.476	1.248
222.27	7102.9	5.035		$21792._3$	6.231	1.245
251.51	8043.0	5.711		$24666._2$	7.049	1.242
273.20	8912.1_5	6.335		$27313._5$	7.803	1.239
293.88	9667.0	6.880		$29612._4$	8.457	1.237
294.71	9696.9	6.901		$29710._8$	8.485	1.237
294.81	9700.7	6.904		$29722._3$	8.488	1.237

Table 4a (cont'd)

Cd #23
$R_o = 1.270(\pm.005)\mu\Omega$

$\theta = 59\tfrac{1}{2}° \ (\pm 1°)$

$(\ell/A)_{295} = 2231.9(\pm 3) \ cm^{-1}$

$B = 0.022(\pm 0.004)$

Cd #7
$R_o = 1.354(\pm.02)\mu\Omega$

$\theta = 36\tfrac{1}{2}° \ (\pm 2°)$

$(\ell/A)_{295} = 1978.1(\pm 4) \ cm^{-1}$

$B = 0.032(\pm 0.004)$

Cd #12
$R_o = 1.177(\pm.005)\mu\Omega$

$\theta = 45° \ (\pm 2°)$

$(\ell/A)_{295} = 2617.8(\pm 4) \ cm^{-1}$

$B = 0.027(\pm 0.004)$

	Cd #23		Cd #7		Cd #12	
Temp	R	ρ_i	R	ρ_i	R	ρ_i
2.18	1.28_3	0.00000_6	–	–	1.18_5	0.00000_3
2.99	1.32_3	0.00002_3	1.40_2	0.00002_4	1.23_5	0.00002_2
4.13	1.52_0	0.00011_0	1.59_2	0.00011_8	1.44_5	0.00010_1
4.20	1.54_0	0.00011_9	1.60_0	0.00012_2	1.46_0	0.00010_6
6.09	3.25_0	0.00086_9	3.11_5	0.00087_6	3.39_0	0.00083_1
7.73	8.10_0	0.00299_8	7.68_0	0.00314_6	9.24_0	0.00302_7
9.89	22.92_0	0.00950_3	22.16_5	0.01035	27.62_0	0.00992_8
13.16	71.97_0	0.03103	71.38_0	0.03482	89.91_0	0.03331
18.86	238.63	0.1042	242.62	0.1200	305.79	0.1144

Tables 4a (cont'd)

Temp.	Cd #23 R	Cd #23 ρ_1	Cd #7 R	Cd #7 ρ_1	Cd #12 R	Cd #12 ρ_1
26.34	570.00$_\sigma$	0.2497	582.03	0.2887	734.12	0.2752
28.66	688.■	.3016	701.40	0.3481	885.10	0.3319
36.92	114■	■06	1150.8$_5$	0.5714	1457.4$_4$	0.5467
47.96	17■■	■53	1779.6	0.8839	2262.7	0.8490
62.02	2636.■	1.■58	2590.6	1.287	3305.6	1.241
76.85	3517.7	1.546	3429.7$_5$	1.704	4385.5	1.646
76.87	3519.1	1.547	3431.6	1.705	4386.9	1.647
76.88	3519.2	1.547	3431.$_5$	1.705	4387.1	1.647
76.94	3523.5	1.549	3435.2	1.706	4392.6	1.649
77.15	3525.0	1.549	3437.0	1.707	4394.0	1.649
77.16	3536.4	1.554	3447.9	1.713	4408.9	1.655
93.67	4517.1	1.987	4382.0	2.177	5611.5	2.107
124.90	6344.6$_5$	2.793	6127.6	3.044	7857.6	2.951
150.54	7839.4	3.455	7559.6	3.755	9698.1	3.644
177.69	9421.4	4.156	9078.7	4.510	11649.$_4$	4.379
197.36	10572.$_5$	4.667	10186.$_5$	5.061	13070.$_0$	4.915
222.27	12043.$_9$	5.321	11602.$_4$	5.765	14883.$_0$	5.599
251.51	13636.$_{35}$	6.031	13135.$_2$	6.528	16847.$_1$	6.341
273.20	15102.$_{65}$	6.685	14545.$_{25}$	7.230	18656.$_{25}$	7.025
293.88	16378.$_3$	7.255	15771.$_6$	7.841	20228.$_7$	7.620
294.71	16431.$_5$	7.279	15822.$_9$	7.866	20294.$_6$	7.645
294.81	16438.$_0$	7.282	15829.$_2$	7.870	20302.$_3$	7.648

Table 4a (cont'd)

Cd #29 $R_O = 1.674(\pm.005)\mu\Omega$

$\theta = 24\tfrac{1}{2}° \ (\pm 1°)$

$(\ell/A)_{295} = 1742.8(\pm 4) \ cm^{-1}$

$B = 0.025(\pm 0.004)$

Cd #27 $R_O = 2.592(\pm.005)\mu\Omega$

$\theta = 34\tfrac{1}{2}° \ (\pm 1°)$

$(\ell/A)_{295} = 3456.0(\pm 5) \ cm^{-1}$

$B = 0.026(\pm 0.004)$

Cd #28 $R_O = 3.607(\pm.005)\mu\Omega$

$\theta = 22\tfrac{1}{2}° \ (\pm 1\tfrac{1}{2}°)$

$(\ell/A)_{295} = 3565.1(\pm 4) \ cm^{-1}$

$B = 0.028(\pm 0.004)$

	Cd #29		Cd #27		Cd #28	
Temp.	R	ρ_i	R	ρ_i	R	ρ_i
2.18	1.68_2	0.00000_5	2.60_8	0.00000_5	3.62_5	0.00000_5
2.99	1.70_7	0.00001_9	2.66_0	0.00001_9	3.67_0	0.00001_7
4.13	1.86_4	0.00010_8	2.97_0	0.00010_8	3.98_2	0.00010_4
4.20	1.86_0	0.00010_6	2.97_0	0.00010_8	3.97_0	0.00010_1
6.09	3.24_0	0.00089_1	5.58_0	0.00085_4	6.78_0	0.00088_2
7.73	7.51_0	0.00332_1	13.61_0	0.00314_9	15.56_0	0.00332_2
9.89	21.09_5	0.01105	39.30_0	0.01049	43.71_5	0.01115
13.16	67.33_0	0.03736	126.68	0.03546	139.71	0.03783
18.86	229.06	0.1294	431.48	0.1226	476.27	0.1314

Table 4a (cont'd)

Temp.	Cd #29 R	ρ_1	Cd #27 R	ρ_1	Cd #28 R	ρ_1
26.34	548.91	0.3113	1035.0_6	0.2950	1141.2	0.3161
28.66	660.60	0.3748	1245.7	0.3552	1373.0	0.3804
36.92	1078.69	0.6125	2042.6_2	0.5828	2239.2_4	0.6209
47.96	1657.7	0.9414	3151.0	0.8992	3435.8	0.9528
62.02	2400.2	1.363	4580.6	1.307	4977.8	1.380
76.85	3165.8	1.797	6057.1	1.729	6546.8_5	1.815
76.87	3167.7_5	1.798	6062.3	1.730	6550.4	1.816
76.88	3167.8_5	1.798	6062.6	1.730	6550.8	1.816
76.94	3170.8_5	1.800	6066.4	1.731	6557.6	1.818
77.15	3171.8	1.801	6067.4	1.731	6559.7	1.818
77.16	3181.8	1.806	6086.6	1.737	6580.4	1.824
93.67	4034.6	2.290	7733.4	2.207	8339.2	2.311
124.90	5629.5_5	3.193	$10804._4$	3.083	$11628._7$	3.220
150.54	6939.3	3.935	$13323._6$	3.801	$14331._0$	3.967
177.69	8330.0	4.722	$16004._0$	4.566	$17199._9$	4.759
197.36	9343.4	5.295	$17949._2$	5.121	$19290._7$	5.337
222.27	$10637._9$	6.027	$20439._0$	5.832	$21963._1$	6.074
251.51	$12040._4$	6.821	$23138._7$	6.603	$24859._2$	6.873
273.20	$13335._7$	7.554	$25626._7$	7.314	$27527._9$	7.610
293.88	$14459._6$	8.190	$27786._2$	7.932	$29845._7$	8.250
294.71	$14508._3$	8.217	$27875._8$	7.958	$29944._4$	8.277
294.81	$14514._0$	8.220	$27886._4$	7.961	$29956._0$	8.280

Table 4a (cont'd)

Cd #24 (Top)

$R_o = 1.180(\pm.005)\,\mu\Omega$

$\theta = 88\ 3/4°\ (\pm 1\tfrac{1}{4}°)$

$(\ell/A)_{295} = 1388.1(\pm 2)\ \text{cm}^{-1}$

$B = 0.024(\pm 0.004)$

Cd #24

$R_o = 2.678(\pm.005)$

$\theta = 88\ 3/4°\ (\pm 1\tfrac{1}{4}°)$

$(\ell/A)_{295} = 2863.7(\pm 5)\ \text{cm}^{-1}$

$B = 0.025(\pm 0.004)$

Temp.	Cd #24 (Top)		Cd #24	
	R	ρ_1	R	ρ_1
2.18	1.19_0	0.00000_7	2.69_0	0.00000_4
2.99	1.21_0	0.00002_1	2.74_0	0.00002_1
4.13	1.36_0	0.00012_6	3.04_1	0.00012_3
4.20	1.35_0	0.00011_9	3.05_0	0.00012_6
6.09	2.47_8	0.00091_0	5.36_5	0.00091_2
7.73	5.51_0	0.00303_4	11.61_0	0.00303_2
9.89	14.32_5	0.00921_2	29.86_0	0.00922_6
13.16	42.57_5	0.02901	88.14_5	0.02901
18.86	136.27	0.09468	281.52	0.09465
26.34	322.85	0.2255	666.56	0.2254
28.66	390.20	0.2728	805.30	0.2726
36.92	651.68	0.4563	1345.0_4	0.4560

Table 4a (cont'd)

Temp.	Cd #24 (Top)		Cd #24	
	R	ρ_1	R	ρ_1
47.96	1031.6	0.7232	2129.5	0.7230
62.02	1534.4	1.077	3166.7	1.076
76.85	2057.3	1.446	4247.3	1.445
76.87	2060.6	1.448	4251.6	1.447
76.88	2059.7	1.447	4250.7	1.447
76.94	2060.7	1.448	4253.9	1.448
77.15	2065.1	1.451	4259.4	1.450
77.16	2071.8	1.456	4273.4	1.454
93.67	2654.1	1.867	5476.4	1.866
124.90	3741.0	2.631	7718.6	2.635
150.54	4625.5	3.265	9545.3	3.264
177.69	5565.1	3.935	$11481._1$	3.932
197.36	6247.6	4.422	$12886._{35}$	4.418
222.27	7115.6	5.044	$14677._2$	5.039
251.51	8057.8_5	5.721	$16620._1$	5.715
273.20	8914.0	6.337	$18401._4$	6.336
293.88	9667.5	6.880	$19957._8$	6.879
294.71	9699.8	6.904	$20021._4$	6.902
294.81	9703.6	6.906	$20029._2$	6.904

Table 4b

$R(\mu\Omega)$, $\rho_1(\mu\Omega\ cm)$ and a_1 as a function of Temperature (K) for pure cadmium specimens used in Run #4

Cd #24 (Top) $R_o = 1.148(\pm.005)\mu\Omega$

$\theta = 88\ 3/4°\ (\pm1\frac{1}{4}°)$

$(\ell/A)_{295} = 1388.9(\pm2)\ cm^{-1}$

$B = 0.024(\pm0.004)$

Cd #25 $R_o = 4.165(\pm.005)\mu\Omega$

$\theta = 8°\ (\pm3°)$

$(\ell/A)_{295} = 3455.3(\pm4)\ cm^{-1}$

$B = 0.026(\pm0.004)$

	Cd #24 (Top)		Cd #25		
Temp.	R	ρ_1	R	ρ_1	a_1
1.72	1.15_0	$.00000_1$	4.17_0	0.00000_1	—
1.90	1.17_2	0.00001_7	4.17_4	0.00000_3	—
2.21	1.17_7	0.00002_0	4.18_1	0.00000_5	—
3.15	1.20_8	0.00004_2	4.23_7	0.00002_1	0.5
4.18	1.32_5	0.00012_4	4.48_0	0.00009_1	0.7_3
4.25	1.35_0	0.00014_2	4.52_0	0.00010_2	0.7_2
4.95	1.59_0	0.00031_0	5.02_5	0.00024_8	0.80
6.04	2.42_0	0.00089_1	7.00_6	0.00081_8	0.91_9
7.18	4.17_0	0.00211_7	11.80_8	0.00220_1	1.04_3
8.00	6.20_0	0.00353_8	17.80_0	0.00392_6	1.11_5

Table 4b (cont'd)

	Cd #24 (Top)		Cd #25		
Temp.	R	ρ_1	R	ρ_1	a_1
9.92	14.46	.0032	43.93	0.01145	1.236
13.17	42.61	0.01064	139.35	0.03892	1.35
16.16	85.34	0.05897	291.36	0.08269	1.44
19.35	146.76	0.1020	514.59	0.1470	1.453
23.09	235.47	0.1642	835.04	0.2392	1.470
27.42	354.20	0.2474	1251.9_4	0.3591	1.464
32.36	504.37	0.3527	1759.4_3	0.5050	1.444
38.09	691.10	0.4837	2366.8_6	0.6796	1.417
45.21	936.50	0.6560	3133.4_3	0.8998	1.382
56.01	1319.1_3	0.9250	4299.6	1.234	1.345
64.55	1619.4	1.136	5208.0	1.495	1.325
76.92	2059.2_5	1.446	6519.9_5	1.871	1.303
76.94	2060.0	1.447	6525.2	1.872	1.303
77.24	2080.0	1.461	6558.0	1.882	1.297
100.11	2875.5_5	2.023	8960.9	2.569	1.279
125.31	3748.7_5	2.641	$11587._7$	3.320	1.265
148.74	4557.1	3.215	$14034._1$	4.018	1.258
173.33	5411.5	3.823	$16630._{25}$	4.758	1.253
201.97	6327.3	4.477	$19416._{25}$	5.552	1.248
223.95	7166.7_5	5.078	$21971._0$	6.280	1.245
250.70	8023.8_5	5.694	$24575._3$	7.021	1.241
273.21	8917.3_5	6.336	$27312._3$	7.800	1.239
293.43	9653.7	6.866	$29558._9$	8.439	1.237
297.51	9805.4	6.976	$30015._8$	8.569	1.236

Table 4c

$R(\mu\Omega)$, $\rho_i(\mu\Omega$ cm) and a_i as functions of Temperature (K)
for pure cadmium specimens used in Run #5

Cd #24 (Bottom) R_o = 1.360 (±.005)$\mu\Omega$

θ = 88 3/4° (±1¼°)

$(\ell/A)_{295}$ = 1391.3(±3) cm^{-1}

B = 0.023(±0.004)

Cd #25 R_o = 4.060(±.005)$\mu\Omega$

θ = 8° (±3°)

$(\ell/A)_{295}$ = 3455.5(±4) cm^{-1}

B = 0.026(±0.004)

	Cd #24 (Bottom)		Cd #25		
Temp.	R	ρ_i	R	ρ_i	a_i
2.07	1.37	0.00000_7	4.07	0.00000_3	–
3.04	1.40	0.00002_8	4.13_5	0.00002_2	0.8
4.18	1.53	0.00011_9	4.38_5	0.00009_4	0.8
4.97	1.78	0.00029_4	4.95	0.00025_6	0.87
6.11	2.68	0.00092_3	7.09	0.00087_2	0.95
7.27	4.57	0.00224_4	12.30	0.00237_3	1.06
8.11	6.72	0.00374_8	18.67_5	0.00420_8	1.13
10.21	16.50	0.01059	49.74	0.01315	1.250
13.48	46.62	0.03165	152.37	0.4270	1.360
16.43	90.34	0.06222	308.44	0.08763	1.420
22.78	227.86	0.1584	806.96	0.2311	1.472

Table 4c (cont'd)

	Cd #24 (Bottom)		Cd #25		
Temp.	R	ρ_1	R	ρ_1	α_1
26.60	331.25	0.2308	1171.9_8	0.3361	1.469
31.47	477.03	0.3328	1668.0_6	0.4788	1.451
36.72	646.21	0.4513	2221.5	0.6378	1.425
43.08	862.39	0.6028	2904.2_3	0.8340	1.395
48.20	1042.1	0.7288	3457.6_7	0.9928	1.373
55.80	1312.6_3	0.9187	4277.2_8	1.228	1.347
65.35	1651.6	1.157	5294.4	1.520	1.323
76.95	2064.8_5	1.448	6522.6_5	1.871	1.302
103.61	3004.1	2.110	9325.1	2.673	1.276
121.71	3632.2_5	2.554	$11211._{05}$	3.212	1.266
136.01	4127.8	2.905	$12705._0$	3.639	1.261
150.75	4636.4	3.266	$14243._3$	4.078	1.257
168.07	5233.7	3.690	$16055._1$	4.594	1.253
184.31	5796.4	4.091	$17765._7$	5.082	1.250
205.55	6533.3_5	4.616	$20012._0$	5.722	1.247
221.64	7093.8	5.017	$21722._7$	6.209	1.245
238.12	7673.6	5.432	$23491._0$	6.712	1.244
255.70	8298.2	5.880	$25399._5$	7.256	1.242
273.18	8930.5	6.334	$27316._5$	7.801	1.239
297.50	9817.7	6.973	$30013._7$	8.568	1.237
298.35	9846.5	6.993	$30111._4$	8.596	1.237
314.36	$10449._0$	7.428	$31933._1$	9.114	1.235
326.95	$10924._9$	7.772	$33378._4$	9.525	1.233

Table 5a

$R(\mu\Omega)$, $\rho_A(\mu\Omega\ cm)$ and $\Delta(\mu\Omega\ cm)$ as functions of Temperature (K) for specimens made from Cd0.76Mg master alloy.

Cd0.76Mg #3

$R_o = 361.355(\pm.005)\mu\Omega$

$\theta = 89\tfrac{1}{2}°\ (\pm1°)$

$(\ell/A)_{295} = 1399.6(\pm3)\ cm^{-1}$

$B = 0.028(\pm0.004)$

Cd0.76Mg #5

$R_o = 715.590(\pm.010)\mu\Omega$

$\theta = 83\tfrac{1}{2}°\ (\pm1°)$

$(\ell/A)_{295} = 2754.3(\pm4)\ cm^{-1}$

$B = 0.030(\pm0.004)$

	Cd0.76Mg #3			Cd0.76Mg #5		
Temp.	R	ρ_A	Δ	R	ρ_A	Δ
1.72	361.36_0	0.2505_{25}	0.00000_7	–	–	–
2.21	361.39_5	0.2505_{49}	0.00001_3	–	–	–
3.15	361.47_9	0.2506_{10}	0.00005_2	715.79_2	0.2519_{89}	0.00003_7
4.18	361.70_0	0.2507_{66}	0.00012_6	716.23_0	0.2521_{46}	0.00011_2
4.25	361.76_4	0.2508_{10}	0.00015_3	716.34_4	0.2521_{86}	0.00013_5
4.95	362.14_3	0.2510_{75}	0.00025_1	717.10	0.2524_{54}	0.00023_7
6.04	363.33_5	0.2519_{04}	0.00050_2	720.08	0.2535_{06}	0.00071_0
7.18	366.81	0.2543_{16}	0.00169_4	726.37	0.2557_{23}	0.00170_5
8.00	–	–	–	733.49	0.2582_{32}	0.00279_5
9.92	384.05	0.2662_8	0.00648	760.56	0.2677_7	0.00655

Table 5a (cont'd)

	Cd0.76Mg #3			Cd0.76Mg #5		
Temp.	R	ρ_A	Δ	R	ρ_A	Δ
13.17	423.60	0.2937_1	0.01429	839.18	0.2954_6	0.01451
16.16	475.38	0.3296_2	0.02042	942.31	0.3317_8	0.02085
19.35	543.44	0.3768	0.0248	1077.8_6	0.3795	0.0255
23.09	636.42	0.4414	0.0275	1262.8_6	0.4447	0.0284
27.42	757.11	0.5252	0.0285	1502.7_2	0.5293	0.0297
32.36	907.79	0.6298	0.0284	1801.7_7	0.6348	0.0298
38.09	1094.5_2	0.7596	0.0278	2171.9_7	0.7654	0.0294
45.21	1338.3_7	0.9292	0.0259	2655.1	0.9360	0.0279
56.01	1720.6	1.195_3	0.0245	3411.8_7	1.203_5	0.0269
64.55	2022.6	1.406	0.024_7	4009.9	1.415	0.027_6
76.92	2463.1_1	1.713	0.023_8	4881.6_9	1.724	0.027_3
76.94	2464.0	1.714	0.023_9	4883.7	1.725	0.027_4
77.24	2485.0	1.729	0.024_6	4903.0	1.732	0.020_3
100.11	3281.6	2.286	0.0228	6502.0_5	2.300	0.027_4
125.31	4157.5	2.900	0.022_0	8236.3_5	2.917	0.027_8
148.74	4968.6	3.471	0.021_4	9842.2	3.490	0.028_3
173.33	5826.0	4.075	0.020_8	$11539._{85}$	4.098	0.028_9
201.97	6744.3_5	4.725	0.019_7	$13357._{85}$	4.751	0.029_0
223.95	7587.1	5.322	0.019_3	$15026._3$	5.351	0.029_7
250.70	8447.5	5.935	0.018_9	$16727._8$	5.966	0.029_8
273.21	9350.8_5	6.578	0.023_0	$18521._1$	6.613	0.036_7
293.43	$10095._3$	7.109	0.026_3	$19994._4$	7.147	0.040_8
297.51	$10245._{05}$	7.216	0.024_5	$20298._6$	7.257	0.041_9

Table 5a (cont'd)

CdO.76Mg #6 $\qquad$ $R_o = 503.035(\pm.005)\mu\Omega$

$\theta = 29° \ (\pm1°)$

$(\ell/A)_{295} = 2269.5(\pm4) \ \text{cm}^{-1}$

$B = 0.022(\pm0.004)$

CdO.76Mg #8 $\qquad$ $R_o = 425.695(\pm.005)\mu\Omega$

$\theta = 16\tfrac{1}{2}° \ (\pm1\tfrac{1}{2}°)$

$(\ell/A)_{295} = 1976.8(\pm4) \ \text{cm}^{-1}$

$B = 0.029(\pm0.004)$

	CdO.76Mg #6			CdO.76Mg #8		
Temp	R	ρ_A	Δ	R	ρ_A	Δ
1.72	–	–	–	425.70_0	0.2136_{10}	
1.90	503.07_5	0.2198_{73}	0.00000_9	425.72_6	0.2136_{23}	0.00000_8
2.21	503.08_8	0.2198_{78}	0.00001_3	425.73_8	0.2136_{29}	0.00001_2
3.15	503.21_1	0.2199_{31}	0.00004_8	425.84_7	0.2136_{82}	0.00004_9
4.18	503.61_0	0.2201_{04}	0.00014_9	426.20_0	0.2138_{58}	0.00015_4
4.25	503.73_5	0.2201_{59}	0.00019_1	426.31_6	0.2139_{16}	0.00020_0
4.95	505.00_0	0.2207_{11}	0.00059_3	427.03_6	0.2142_{75}	0.00041_3
6.04	507.56_0	0.2218_{25}	0.00113_6	429.88_0	0.215●_{97}	0.00126_5
7.18	514.15_0	0.2247_{04}	0.00267_1	435.95_0	0.2187_{40}	0.00293_9
8.00	521.50	0.2279_{15}	0.00422_8	442.81	0.2221_{81}	0.00467_7
9.92	–	–	–	468.84	0.2352_4	0.01034
13.17	–	–	–	544.77	0.2733_2	0.02150

Table 5a (cont'd)

Temp.	Cd0.76Mg #6 R	ρ_A	Δ	Cd0.76Mg #8 R	ρ_A	Δ
16.16	–	–	–	645.50	0.3238_5	0.02924
19.35	–	–	–	778.48	0.3906	0.0332
23.09	–	–	–	958.49	0.4808	0.0333
27.42	–	–	–	1187.0	0.5953	0.0305
32.36	–	–	–	1463.6_3	0.7339	0.0260
38.09	–	–	–	1795.5_3	0.9001	0.0208
45.21	–	–	–	2216.4_5	1.110_7	0.0149
56.01	–	–	–	2860.2	1.432_6	0.0071
64.55	3719.3	1.623	-0.008_4	3363.4	1.684	0.001_9
76.92	4525.8_3	1.975	-0.017_2	4092.5_5	2.048	-0.004_8
76.94	4528.3	1.976	-0.017_4	4095.3	2.050	-0.004_8
77.24	4553.0	1.987	-0.017_0	4129.0	2.066	0.002_3
100.11	6028.5	2.629	-0.032_2	5451.8	2.726	-0.015_6
125.31	7645.9_5	3.334	-0.047_2	6916.2_5	3.456	-0.026_2
148.74	9151.5	3.989	-0.060_8	8280.0	4.135	-0.035_8
173.33	$10749._{35}$	4.685	-0.074_4	9728.0_5	4.856	-0.045_3
201.97	$12464._5$	5.431	-0.088_6	$11283._{65}$	5.629	-0.054_7
223.95	$14041._{05}$	6.118	-0.099_9	$12713._8$	6.341	-0.061_4
250.70	$15649._{65}$	6.818	-0.110_8	$14175._6$	7.067	-0.066_2
273.21	$17340._3$	7.555	-0.121_1	$15707._2$	7.829	-0.073_3
293.43	$18730._4$	8.160	-0.128_9	$16968._8$	8.456	-0.077_1
297.51	$19014._3$	8.284	-0.130_3	$17224._6$	8.583	-0.078_3

Table 5b

$R(\mu\Omega)$, $\rho_A(\mu\Omega \text{ cm})$ and $\Delta(\mu\Omega \text{ cm})$ as functions of Temperature (K) for specimens made from Cd1.5Mg master alloy.

Cd1.5Mg #3 $R_0 = 1462.055(\pm.005)\mu\Omega$

$\theta = 29\frac{1}{2}° \ (\pm 1\frac{1}{2}°)$

$(\ell/A)_{295} = 3441.3(\pm 9) \text{ cm}^{-1}$

$B = 0.032(\pm 0.004)$

Cd1.5Mg #4 $R_0 = 1219.120(\pm.005)\mu\Omega$

$\theta = 54°(\pm 1°)$

$(\ell/A)_{295} = 2739.1(\pm 7) \text{ cm}^{-1}$

$B = 0.029(\pm 0.004)$

	Cd1.5Mg #3			Cd1.5Mg #4		
Temp.	R	ρ_A	Δ	R	ρ_A	Δ
2.07	1462.0_8	0.4190_{96}	–	1219.1_4	0.4353_{36}	0.00000_4
3.04	1462.2_4	0.4191_{20}	0.00002_4	1219.3_{15}	0.4354_{00}	0.00004_8
4.18	1463.0_9	0.4193_{81}	0.00018_9	1220.0_1	0.4356_{49}	0.00021_4
4.97	1464.8_2	0.4198_{73}	$.00051_5$	1221.3_8	0.4361_{41}	0.00053_6
6.11	1470.5_8	0.4215_{17}	0.00154_3	1225.7_9	0.4377_{13}	0.00148_6
7.27	1482.9_2	0.4250_{52}	0.00362_3	1235.1_6	0.4410_{60}	0.00345_4
8.11	1496.6_2	0.4289_{77}	0.00579_2	1245.4_7	0.4447_{43}	0.00552_3
10.21	1553.6_5	0.4453_1	0.01369	1288.0_2	0.4599_4	0.01317
13.48	1701.4_7	0.4876_7	0.02851	1396.7_5	0.4987_7	0.02804
16.43	$188?._4$	0.5403_0	0.03960	1529.6_9	0.5462_4	0.04002

Table 5b (cont'd)

Temp.	Cd1.5Mg #3 R	ρ_A	Δ	Cd1.5Mg #4 R	ρ_A	Δ
22.78	2384.7_1	0.6834	0.0504	1885.8_1	0.6734	0.0548
26.60	2727.2_2	0.7815	0.0512	2129.3_9	0.7605	0.0583
31.47	3186.7_6	0.9130	0.0497	2458.5_1	0.8781	0.0600
36.72	3698.9_9	1.059_6	0.0469	2828.6_9	1.010_3	0.0600
43.08	4333.6_4	1.241_2	0.0431	3291.7_5	1.175_9	0.0590
48.20	4850.7_7	1.389_2	0.0400	3671.7_5	1.311_7	0.0578
55.80	5619.3_3	1.608_9	0.0357	4239.4_3	1.5	0.0558
65.35	6572.3	1.881	0.029_5	4945.7_5	1.76	0.052_6
76.95	7734.8	2.214	0.024_8	5808.4	2.076	0.050_5
103.61	$10380._3$	2.969	0.012_9	7768.4	2.779	0.044_5
121.71	$12159._{25}$	3.478	0.005_2	9082.3_5	3.250	0.040_5
136.01	$13567._5$	3.880	-0.000_8	$10120._7$	3.623	0.037_4
150.75	$15017._9$	4.294	-0.006_5	$11188._{05}$	4.007	0.034_3
168.07	$16726._{35}$	4.782	-0.012_9	$12444._1$	4.459	0.031_2
184.31	$18340._1$	5.242	-0.018_5	$13629._7$	4.886	0.028_7
205.55	$20460._4$	5.848	-0.025_2	$15186._5$	5.447	0.026_4
221.64	$22077._1$	6.310	-0.029_5	$16373._0$	5.876	0.025_4
238.12	$23752._8$	6.788	-0.032_7	$17604._2$	6.321	0.025_9
255.70	$25563._5$	7.306	-0.035_3	$18933._7$	6.802	0.027_2
273.18	$27388._7$	7.827	-0.036_8	$20274._{75}$	7.287	0.028_4
297.50	$29968._0$	8.565	-0.035_3	$22170._5$	7.974	0.034_4
298.35	$30065._{35}$	8.592	-0.033_5	$22238._1$	7.999	0.035_8
314.36	$31806._5$	9.090	-0.033_3	$23523._3$	8.465	0.040_1
326.95	$33195._6$	9.487	-0.030_5	$24543._8$	8.836	0.044_9

Table 5b (cont'd

Cd1.5Mg #1 $R_o = 1215.410(\pm.005)\,\mu\Omega$

$\theta = 68° \ (\pm 1\tfrac{1}{2}°)$

$(\ell/A)_{295} = 2749.8(\pm 6)\ \mathrm{cm}^{-1}$

$B = 0.033(\pm 0.004)$

Cd1.5Mg #2 $R_o = 1352.615(\pm.005)\,\mu\Omega$

$\theta = 87° \ (\pm 1\tfrac{1}{2}°)$

$(\ell/A)_{295} = 3503.0(\pm 7)\ \mathrm{cm}^{-1}$

$B = 0.031(\pm 0.004)$

	Cd1.5Mg #1			Cd1.5Mg #2		
Temp.	R	ρ_A	Δ	R	ρ_A	Δ
2.07	1215.4_{55}	0.4292_{33}	0.00001_6	1352.6_6	0.3967_{66}	0.00001_4
3.04	1215.6_7	0.4293_{12}	0.00007_4	1353.0_{35}	0.3968_{80}	0.00010_7
4.18	1216.4_6	0.4295_{94}	0.00026_9	1354.3_2	0.3972_{61}	0.00039_8
4.97	1217.8_9	0.4301_{05}	0.00060_8	1356.6_4	0.3979_{49}	0.00091_2
6.11	1222.7_1	0.4318_{06}	0.00168_4	1363.9_5	0.4000_{93}	0.00243_1
7.27	1232.7_2	0.4353_{44}	0.00388_2	1378.8_0	0.4044_{54}	0.00547_5
8.11	1243.6_{85}	0.4392_{20}	0.00621_4	1394.6_8	0.4091_{16}	0.00864_1
10.21	1288.4_0	0.4550_2	0.01490	1457.3_0	0.4274_9	0.02021
13.48	1400.2_0	0.4945_1	0.03222	1604.9_5	0.4708_2	0.04256
16.43	1533.8_6	0.5417_3	0.04696	1772.1_4	0.5198_8	0.06116
22.78	1883.4_4	0.6653	0.0680	2189.8_8	0.6425	0.0880
26.60	2119.9_3	0.7489	0.0750	2466.5_1	0.7238	0.0972

Table 5b (cont'd)

Temp.	Cd1.5Mg #1			Cd1.5Mg #2		
	R	ρ_A	Δ	R	ρ_A	Δ
31.47	2438.4_7	0.8616	0.0803	$283?\ 2_3$	0.8328	0.1045
36.72	2797.2	0.9885	0.0835	3254.5_3	0.9556	0.1093
43.08	3246.9_7	1.147_7	0.0855	3778.4_6	1.109_8	0.1126
48.20	3616.7_7	1.278_7	0.0864	4209.9_7	1.236_9	0.1142
55.80	4169.9_5	1.474_8	0.0870	4856.1_3	1.427_3	0.1157
65.35	4858.6_5	1.719	0.086_6	5661.3	1.665	0.116_2
76.95	5700.0	2.018	0.087_3	6644.9	1.956	0.117_4
103.61	7609.0	2.697	0.087_3	8874.3_5	2.616	0.118_3
121.71	8886.6_5	3.152	0.087_2	$10364._{25}$	3.058	0.118_6
136.01	9886.3	3.509	0.084_0	$11539._7$	3.408	0.118_9
150.75	$10931._8$	3.883	0.087_4	$12746._1$	3.767	0.119_1
168.07	$12150._6$	4.319	0.088_0	$14164._0$	4.191	0.119_8
184.31	$13301._{05}$	4.732	0.089_3	$15501._2$	4.590	0.120_7
205.55	$14811._{05}$	5.274	0.091_9	$17255._9$	5.116	0.123_1
221.64	$15962._3$	5.688	0.094_8	$18592._8$	5.517	0.125_5
238.12	$17155._6$	6.117	0.098_8	$19979._1$	5.934	0.129_1
255.70	$18445._8$	6.583	0.104_6	$21477._6$	6.385	0.134_4
273.18	$19744._{05}$	7.052	0.108_3	$22990._{35}$	6.842	0.138_5
297.50	$21583._0$	7.717	0.119_5	$25127._9$	7.488	0.148_8
298.35	$21645._6$	7.739	0.120_5	$25199._{85}$	7.510	0.149_9
314.36	$22895._4$	8.192	0.128_8	$26654._0$	7.950	0.157_6
326.95	$23884._2$	8.551	0.135_8	$27804._4$	8.299	0.164_2

CHAPTER 5
DISCUSSION OF RESULTS

5.1 Electrical Resistivity of Pure Cadmium

We present new results for the electrical resistivity of Cd which represent the first systematic investigation since 1932. Our values for the ice point (273.15 K) resistivities are $\rho_{1||} = 7.81(\pm 0.03)\mu\Omega$ cm and $\rho_{1\perp} = 6.30(\pm 0.03)\mu\Omega$ cm, the uncertainties being primarily due to the scatter of points on the plot of $\rho_{1273}(\theta)$ versus $\cos^2\theta$ shown in Fig. 2. The various values of ice point resistivities of Cd are summarized below:

Author	R_{295}/R_o	$\rho_{1\|\|273}$ ($\mu\Omega$ cm)	$\rho_{1\perp273}$ ($\mu\Omega$ cm)
this work	1×10^4	7.81 03)	6.30($\pm$0.03)
Bridgman (1925)		7.68($\pm$0.1)	6.30($\pm$0.1)
Bridgman (1929)		7.62($\pm$0.05)	6.32($\pm$0.05)
Grüneisen and Goens (1923)		7.79	6.55
Grüneisen and Goens (1924)		7.79	6.54
Goens and Grüneisen (1932)		7.73	6.36$_5$
cited in Meaden (1965)		7.73	6.35

Bridgman's measurements were made at 20°C and have been adjusted to the ice point. His uncertainties have been inferred from the scatter of his points on a graph of ρ
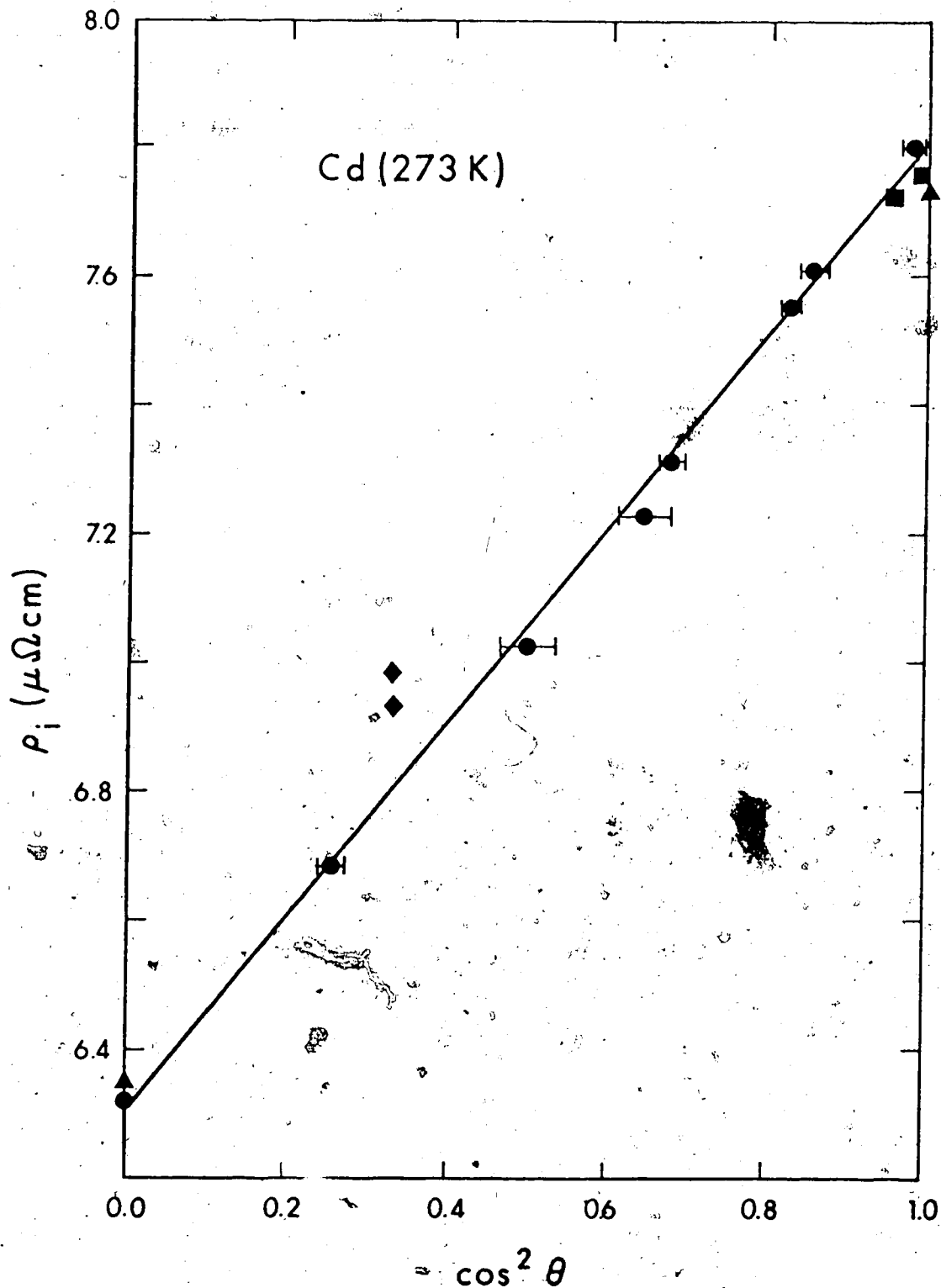
Fig. 2. Ideal resistivities ρ_i versus $\cos^2\theta$ for pure Cd at 273.15 K. ● - this work, ▲ - cited in Meaden (1965), ■ - Alderson and Hurd (1975), ◆ - polycrystalline values from Seth (1969).

versus $\cos^2\theta$. All three of the studies by Grüneisen and Goens appear to be based on two or more of the same four single crystals. The values cited in Meaden can be traced back to a review article by Grüneisen (1945) who in turn attribute those values to Goens and Grüneisen but does not give specific reference.

Alderson and Hurd (1975) appear to have done a systematic study of the resistivity of Cd, but although they plot graphs of $\rho_{i||}$ and $\rho_{i\perp}$ as functions of temperature and they do quote a value for the high temperature limit of the ideal resistivity anisotropy = 1.214, they do not quote actual values for $\rho_{i||273}$ and $\rho_{i\perp273}$. This is an unfortunate omission if, in fact, they did calculate accurate values. (We also note that qualitative conclusions they draw do not depend on highly accurate resistivity measurements). They do however give ice point resistivities for two of their single crystal specimens, both of which have orientations close to parallel ($\theta = 0°$) and these have been included in Fig. 2. Recent comparable data for the axial resistivities would, however, have been valuable.

In Fig. 3, electrical resistivities at 26.34 K are plotted against $\cos^2\theta$. Here, the anisotropy ratio $a_{126} = 1.470$ is considerably larger than its ice point value $a_{1273} = 1.239$. Note that the positions of these points relative to the straight line is almost identical to their relative positions in Fig. 2, indicating that the
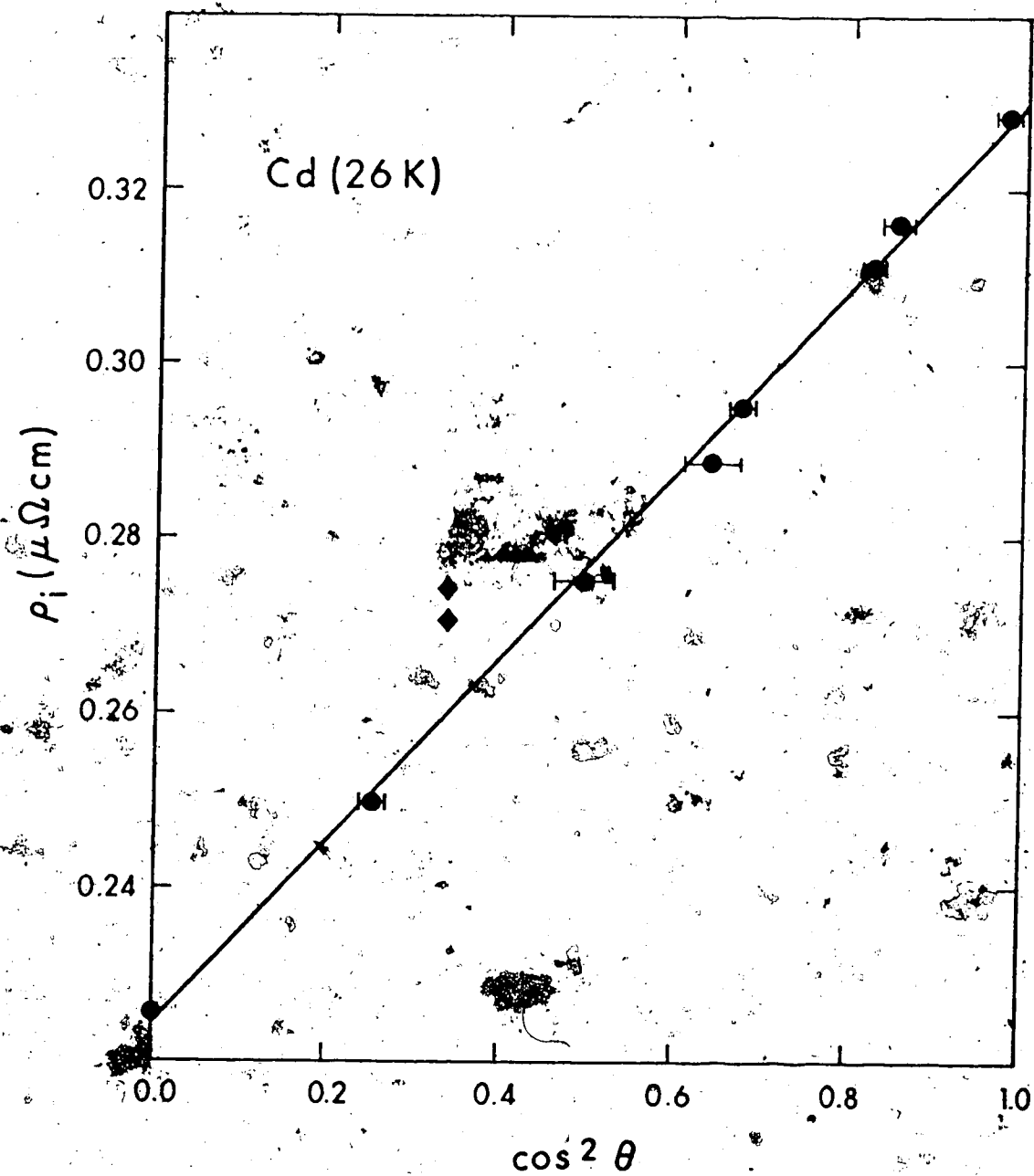
Fig. 3. Ideal resistivities ρ_i versus $\cos^2\theta$ for pure Cd at 26.34 K. ●— this work, ◆— polycrystalline values interpolated from tables in Seth (1969).

scatter of the points about the line is largely due to random errors in the determination of orientations (shown by the horizontal error bars) as opposed to random errors in the resistivity values.

ρ_{126} has been plotted against ρ_{1273} for each pure Cd specimen in Fig. 4 for two reasons:

First, this graph also helps to ascertain whether or not there are significant random errors in the electrical resistivities. If the resistivities are accurate, all points should lie on the same straight line independent of their orientation determinations. (Actually, the very small change of orientation on thermal contraction causes the line to be slightly concave upwards, the maximum deviation from linearity being approximately equal to the width of the line). The position along the line should be proportional to $\cos^2\theta$, so that an error in θ would cause a point to lie in a slightly different position than expected, but still on the line. Because of the different anisotropies however, random errors in the resistivities produce a scatter of the points about the line. Changing an ℓ/A value by 1% for example would cause a point to move about 1.6 mm off the line in Fig. 4. The low scatter of our points indicates that the random errors in the resistivities were 0.5% or less, as expected. Also, allowing for the probable error in determining θ's, all specimens were in their expected positions along the
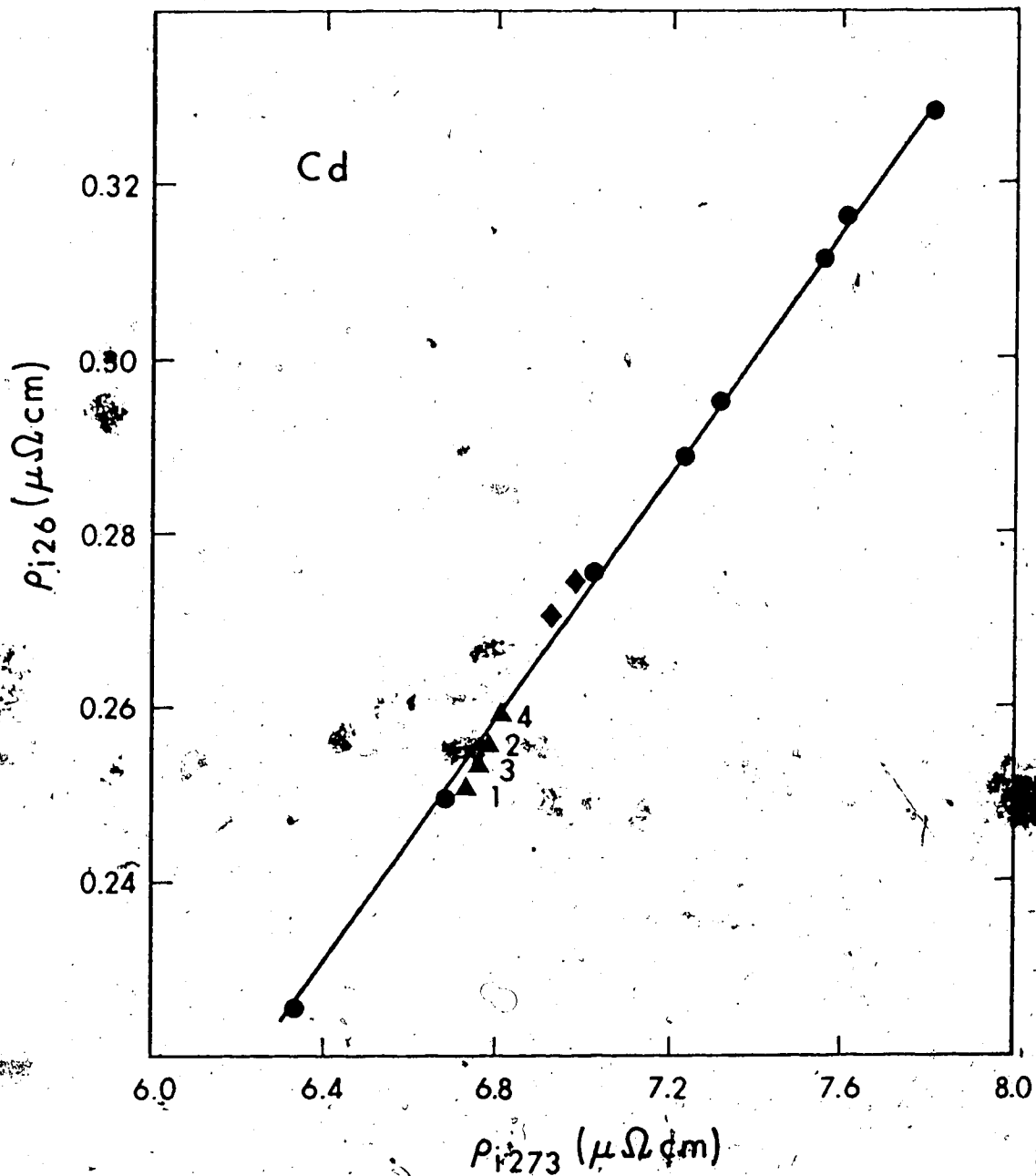
Fig. 4. Ideal resistivities at 26.34 K (ρ_{126}) versus ideal resistivities at 273.15 K (ρ_{1273}) for pure Cd. ● - this work, ◆ - polycrystalline values from Seth (1969), $\blacktriangle_1$, $\blacktriangle_2$, $\blacktriangle_3$ and $\blacktriangle_4$ are calculated polycrystalline values using equations 5.1, 5.2, 5.3 and 5.4 respectively.

line except Cd #7 which was just outside the expected range.

Secondly, Fig. 4 is a useful tool for comparing single crystal electrical resistivities to polycrystalline values. Alstad, Colvin and Legvold (1961) tested four different formulas comparing ρ_{poly} $(= 1/\sigma_{poly})$ to $\rho_{||}$ $(= 1/\sigma_{||})$ and $\rho_{\perp}$ $(= 1/\sigma_{\perp})$:

$$\sigma_{poly} = (1/3)\sigma_{||} + (2/3)\sigma_{\perp} \tag{5.1}$$

$$\rho_{poly} = \frac{[\rho_{\perp}(\rho_{||}-\rho_{\perp})]^{\frac{1}{2}}}{\tan^{-1}\{[(\rho_{||}-\rho_{\perp})/\rho_{\perp}]^{\frac{1}{2}}\}} \tag{5.2}$$

$$\sigma_{poly} = \frac{1}{4}\{\sigma_{\perp} + [\sigma_{\perp}(8\sigma_{||}+\sigma_{\perp})]^{\frac{1}{2}}\} \tag{5.3}$$

$$\rho_{poly} = (1/3)\rho_{||} + (2/3)\rho_{\perp}. \tag{5.4}$$

Although they conclude that for highly anisotropic Yttrium $(\rho_{\perp}/\rho_{||} = 2.07$ at 300 K) Eq. 5.4 is the best, the purity of their specimens was not good (ρ_{300}/ρ_{0} ranged from 6 to 28). It would be worthwhile to repeat this test with a metal for which high purity material is available, such as Sn, even though its anisotropy ratio $a = \rho_{||}/\rho_{\perp}$ is not as extreme.

ρ_{poly} has been calculated using all four of the above formulas with our values of $\rho_{||}$ and $\rho_{\perp}$ at both 273 K and 26 K. These four points have been plotted in Fig. 4, as

well as points for Seth's (1969) two polycrystalline Cd specimens. Although more valid comparison would be possible by measuring the polycrystal and single crystal resistivities simultaneously (ρ_{poly26} was determined by interpolating resistivities Seth has given in tables), both of Seth's specimens appear to have preferred orientations closer to parallel than expected for any of the four formulas.

If we assume that Eq. 5.4 is correct, then a polycrystalline specimen would have the same resistivity as a single crystal with an orientation such that $\cos^2\theta_{293} = 1/3$ (and $\cos^2\theta_{26} = 0.338$). The resistivities of Seth's specimens have therefore been plotted in Figs. 2 and 3 using the above values for the abscissa. These points all lie significantly above the line, indicating again preferred orientations closer to parallel than expected.

We ultimately wish to compare our values of DMR in single crystals to those of Seth and Woods (1970) for polycrystalline specimens. Because Seth and Woods suspected the unusual behaviour in their Cd and Cd-Mg specimens may be due to different preferred orientations in different specimens, it is valuable to determine whether or not preferred orientations do exist.

5.2 Electrical Resistivity of Cd-Mg Alloys

The electrical resistivity of single crystals of an alloy with fixed concentration should also vary as $\cos^2\theta$. Figs. 5 and 6 show the good fits of the ice point resistivities and the residual resistivities to $\cos^2\theta$ for the Cd0.76Mg specimens. ρ_{Ao} is also plotted against ρ_{A273} for these specimens in Fig. 7 and as in Fig. 4 for pure Cd, a straight line is expected providing the resistivities have no large random errors and in the case of alloys providing the impurity concentration does not vary randomly among specimens. A point is plotted for Seth's Cd0.75Mg polycrystalline specimen and it is considerably below the line. This is caused largely if not totally by its lower Mg concentration (~ 0.73 at. % based on the fit to $x(1-x)$ of data in Table 1) compared to our Cd0.76Mg specimens (~ 0.78 at. %, Table 2). An increase in Mg concentration would move that point primarily vertically although also slightly to the right on Fig. 7. With the adjustment for concentration, Seth's point lies to the right of the three points (triangles) calculated using Eqs. 5.1, 5.3 and 5.4, indicating again a preferred orientation closer to parallel than expected. This preferred orientation is confirmed in Fig. 5 where the polycrystalline point lies above the line for the single crystals.

The residual resistivities for the Cd1.5Mg single crystals (which have not been plotted) do not fit well on
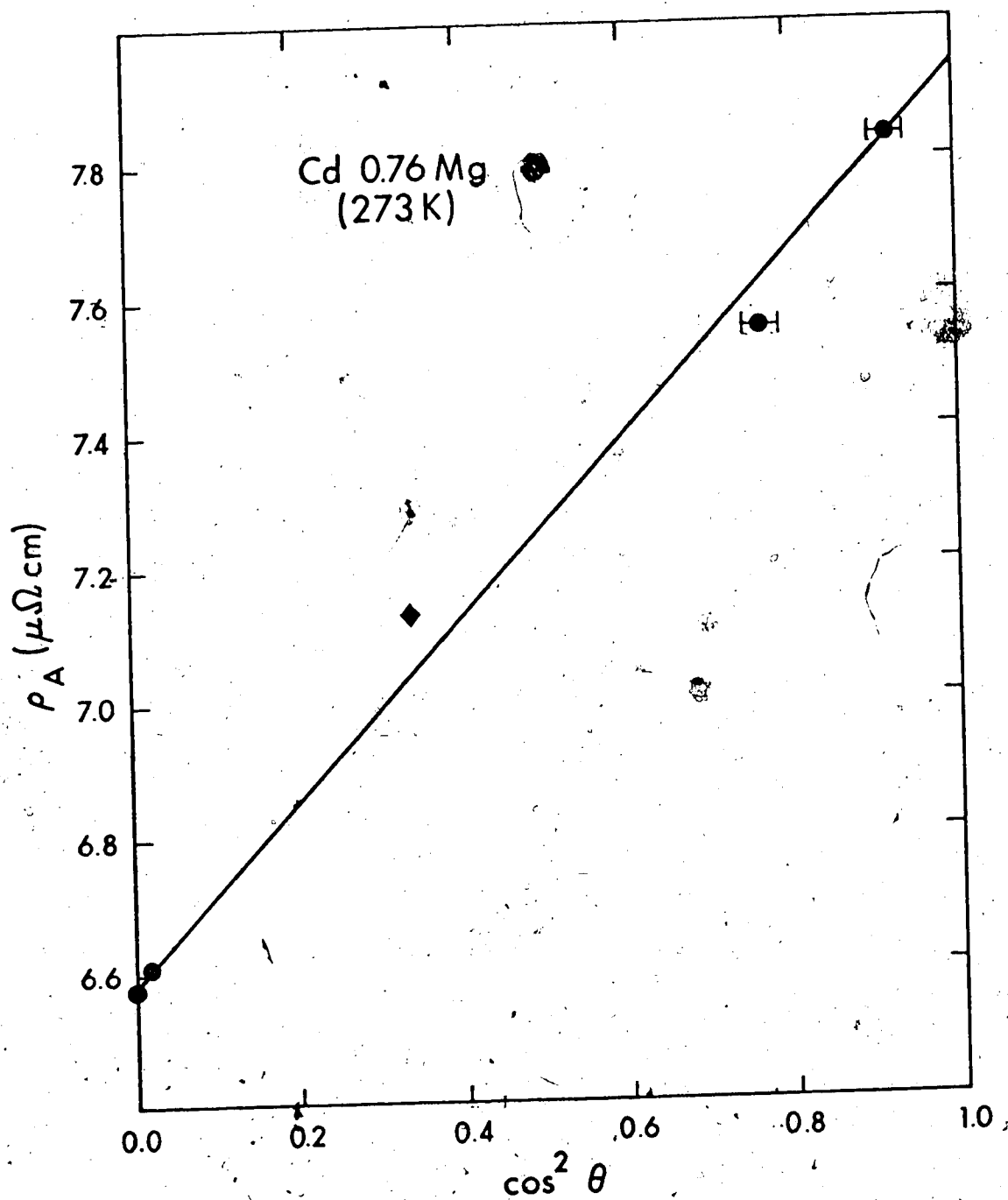
Fig. 5. Alloy resistivities ρ_A versus $\cos^2\theta$ for Cd0.76Mg at 273.15 K. ● - this work, ♦ - polycrystalline value from Seth (1969) for Cd0.75Mg.
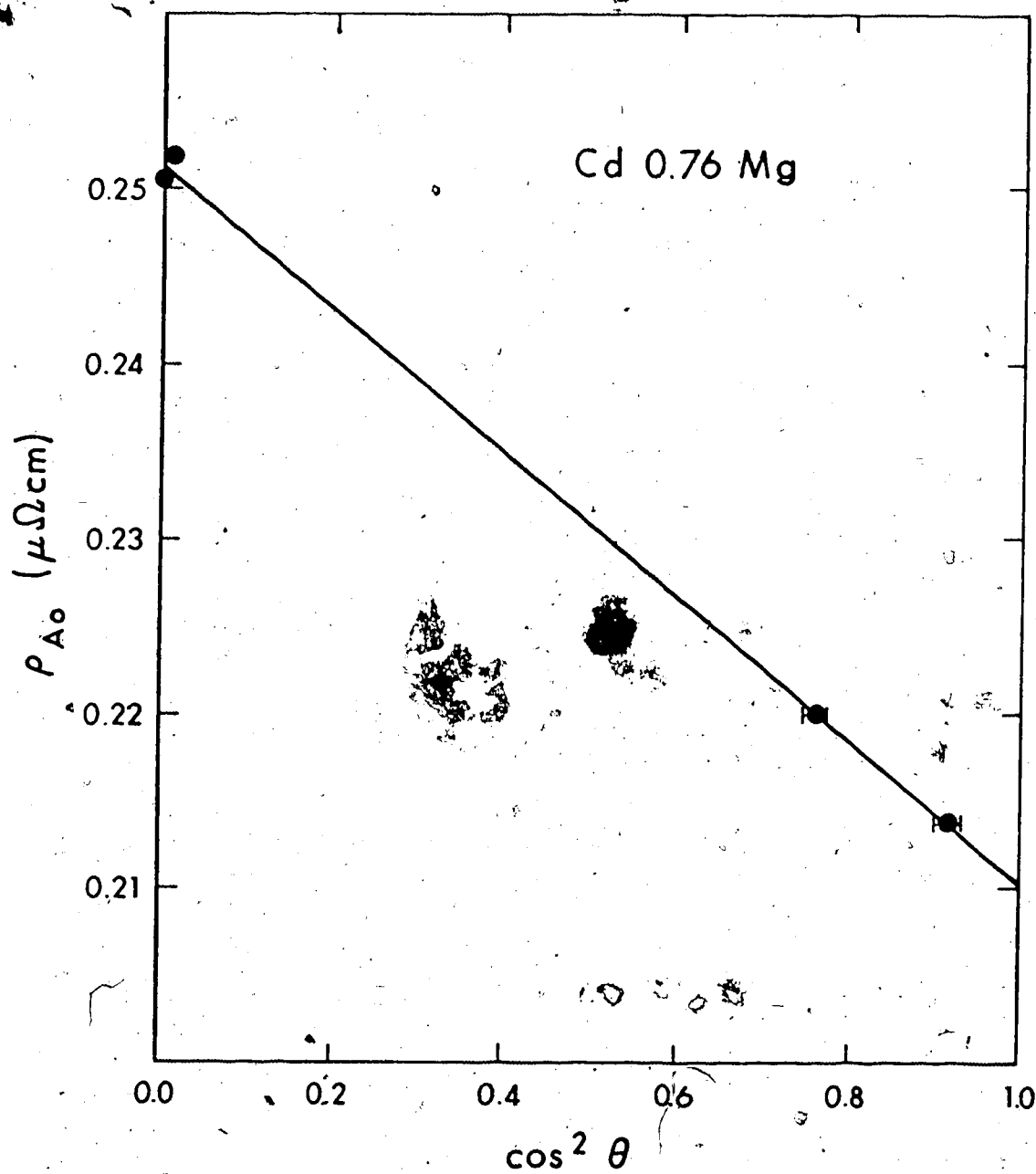
Fig. 6. Alloy residual resistivities ρ_{Ao} versus $\cos^2\theta$
for Cd0.76Mg. ● - this work, ◆ - polycrystalline
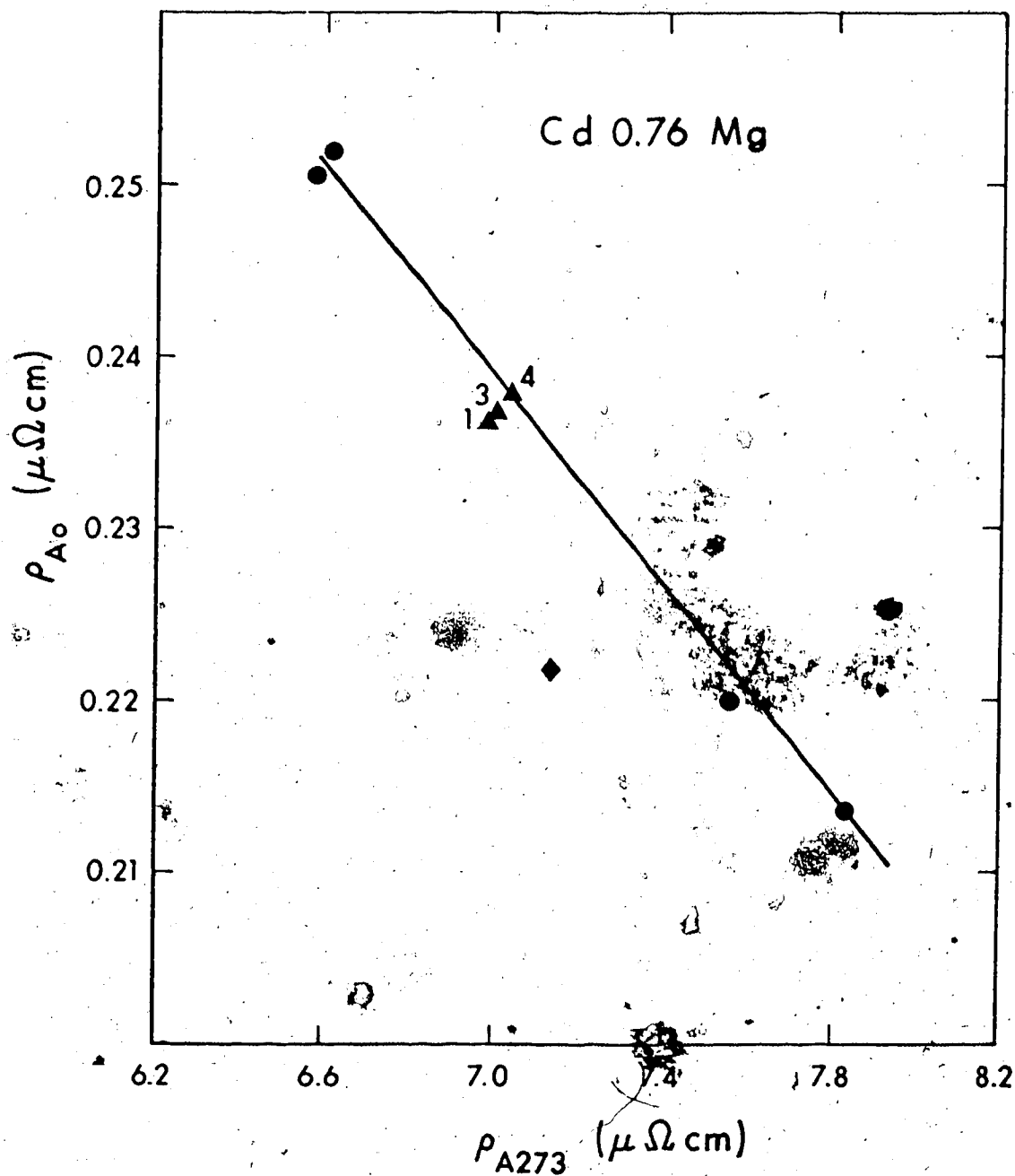value from Seth (1969) for Cd0.75Mg.

Fig. 7. Alloy residual resistivities (ρ_{Ao}) versus alloy resistivities at 273 K (ρ_{A273}) for Cd0.76Mg. ●- this work, ◆- polycrystalline values from Seth (1969) for Cd0.75Mg, ▲$_1$, ▲$_3$ and ▲$_4$ are calculated polycrystalline values using equations 5.1, 5.3 and 5.4 respectively.

a plot against $\cos^2\theta$, probably because of variation from specimen to specimen of the Mg concentration in solid solution. However, the fit of the Cd1.5Mg ice point resistivities (which are relatively weakly dependent on concentration) to $\cos^2\theta$ is good, similar to Fig. 5 (the Cd1.5Mg plot is also not shown explicitly). The position of Seth's Cd1.5Mg polycrystalline specimen, adjusted slightly for concentration differences, is again above the line for the Cd1.5Mg single crystals, again indicating a preferred orientation somewhat closer to parallel than expected.

5.3 Resistivity Anisotropy Ratios

For pure Cd, the ideal resistivity anisotropy ratio $a_i = \rho_{i||}/\rho_{i\perp}$ was calculated at all temperatures as described in Sec. 4.1.5. As Rowlands, Stackhouse and Woods (1975) have shown, the fit of these data with the theoretical calculations of White and Carbotte (1975) for Zn (which has a similar c/a ratio and Brillouin zone structure to Cd) is good. Fig. 8 also shows this comparison, this time including points plotted from three different experimental runs and including the correction to $f = \ell/A$ for thermal expansion (this correction leaves a_{293} unchanged while increasing a_{26} by about 2.4% but does not change the basic shape of the curve). The temperature dependence of a_i agrees well with values measured by Goens
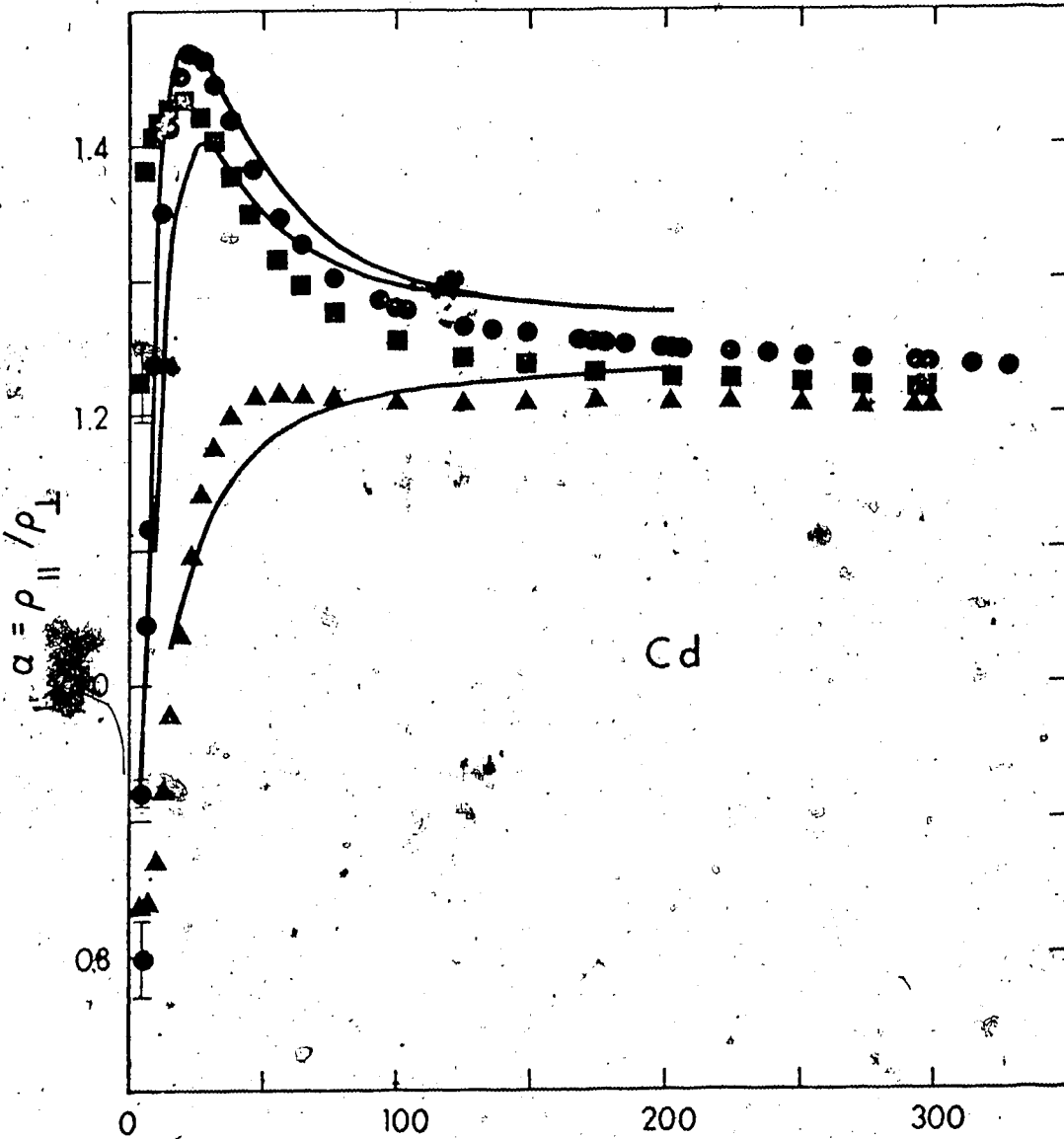
Fig. 8. Resistivity anisotropy ratios $a = \rho_{||}/\rho_{\perp}$ versus temperature T. $\bullet - a_i = \rho_{i||}/\rho_{i\perp}$ for pure Cd, $\blacktriangle - a_A = \rho_{A||}/\rho_{A\perp}$ for Cd0.76Mg, $\blacksquare - (\rho_{A||T}-\rho_{A||o})/(\rho_{A\perp T}-\rho_{A\perp o})$ for Cd0.76Mg. $\rho_o \sim \rho_{iT}$ at 6 K for pure Cd, $\rho_{Ao} \sim \rho_{iT}$ at 23 K for Cd0.76Mg. The solid curves are the theoretical calculations by White and Carbotte (1974) for (from top to bottom) (a) $a_i = \rho_{i||}/\rho_{i\perp}$ for pure Zn (b) $(\rho_{A||T}-\rho_{A||o})/(\rho_{A\perp T}-\rho_{A\perp o})$ for a Zn alloy with $\rho_{Ao} = 0.5\mu\Omega$ cm and (c) $a_{AT} = \rho_{A||T}/\rho_{A\perp T}$ for the same Zn alloy.

and Grüneisen (1932) at 21.2 K, 83.2 K and 273.2 K as well as values of Alderson and Hurd (1975) from 3 K to 590 K.

Our measurements show reasonable qualitative agreement with the predictions of Case and Gueths (1970) (see Sec. 2.1) for any axial metal except at the lowest-temperatures where the measured values of a_{1T} drop well below $a_{1\infty}$. Indeed, Case and Gueths' measurements on Sn lacked the accuracy necessary to test their own low temperature prediction.

White and Carbotte (1974) also calculated the resistivity anisotropy ratio for dilute Zn alloys. Their anisotropy curves for a Zn alloy with a residual resistivity of 0.5μΩ cm and our experimental anisotropy ratios for Cd0.76Mg with residual resistivites of $\sim$ 0.23μΩ cm are also shown in Fig. 8 both with and without the residual resistivities subtracted from the total resistivities. The axial resistivities for Cd0.76Mg were determined using the method described in Sec. 4.1.5 for pure Cd. The straight lines in Figs. 5 and 6 pass through the point for Cd0.76Mg #8 and half way between the points for Cd0.76Mg #3 and Cd0.76Mg #5. The vertical intercepts of these lines determine the axial resistivities. At other temperatures, $\rho_{A||T}$, $\rho_{A\perp T}$ and hence $a_{AT} = \rho_{A||T}/\rho_{A\perp T}$ and $(\rho_{A||T} - \rho_{A||o})/(\rho_{A\perp T} - \rho_{A\perp o})$ were calculated assuming the same fit for these three specimens.

The agreement between experimental and theoretical

anisotropy ratios is not as good for the alloys as for the pure metals. For example the maximum value of $(\rho_{||}-\rho_o)/(\rho_{\perp}-\rho_o)$ occurs at a slightly lower temperature than a_{imax} for the Cd alloys (experiment) but at a slightly higher temperature for the Zr alloys (theory). Admittedly, White and Carbotte have obtained an isotropic residual resistivity which is not the case for Cd0.76Mg alloys (Fig. 6), so one cannot expect to compare these curves in too much detail.

Note that the temperature dependence of all three calculated anisotropies is largely independent of the fits of ρ to $\cos^2\theta$ shown in Figs. 2, 3, 5 and 6. Errors in $\rho_{||}$ and/or $\rho_{\perp}$ could affect the absolute values of the anisotropy ratios but they would not affect the shape of these curves. Even the position of the maximum of $(\rho_{A||T} - \rho_{A||o})/(\rho_{A\perp T} - \rho_{A\perp o})$ (which is the same as $(\rho_{i||T} + \Delta_{||T})/(\rho_{i\perp T} + \Delta_{\perp T})$) relative to a_{imax} will be roughly independent of these fits (Figs. 9 and 10 in the next section show that $\Delta_{||}$ and $\Delta_{\perp}$ are not strongly dependent on concentration and hence ρ_o).

White and Carbotte emphasize that the anisotropy curves for the metal and $(\rho_{||}-\rho_o)/(\rho_{\perp}-\rho_o$ for the alloys are not coincident, indicating that DMR exist. Because they are so sensitive to small changes in ρ, DMR offer a particularly rigorous test of theoretical calculations. DMR are discussed in the following section.

5.4 Deviations from Matthiessen's Rule

Deviations from Matthiessen's rule (DMR or Δ) have been calculated for each single crystal alloy specimen as described in Sec. 4.1.5 and are plotted against temperature in Fig. 9 for Cd0.76Mg specimens and in Fig. 10 for Cd1.5Mg specimens. The bold broken lines enveloping the triangles in Fig. 9 indicate the probable error. Because DMR are calculated by subtracting quantities which are nearly equal ($\rho_{iT} \simeq \rho_{AT} - \rho_{Ao}$), relatively small errors in ρ_{AT}, ρ_{Ao} and ρ_{iT} produce much larger relative errors in Δ.

The values of Δ at 273K for all eight alloy crystals are plotted against $\cos^2\theta$ in Fig. 11. Because ρ_{AT}, ρ_{Ao} and ρ_{iT} are all linear in $\cos^2\theta$, Δ should be linear in $\cos^2\theta$ as well (Eqs. 2.8a and 2.8b). Although greater accuracy would make these results more convincing, Fig. 11 does indeed show that linear relationship with the line for the Cd1.5Mg alloys slightly higher than the line for the Cd0.76Mg alloys. Because Δ was evaluated separately for each alloy specimen, the fit of Δ to $\cos^2\theta$ will not depend greatly on a good fit of ρ_{Ao} to $\cos^2\theta$ (which is not good for Cd1.5Mg).

At the lowest temperatures, $T \lesssim 10K$, Δ follows a power law, $\Delta \propto T^n$ and n was found to be 5.25($\pm$0.2) for the parallel orientation and 4.75($\pm$0.2) for the perpendicular orientation. These values are consistent with the value
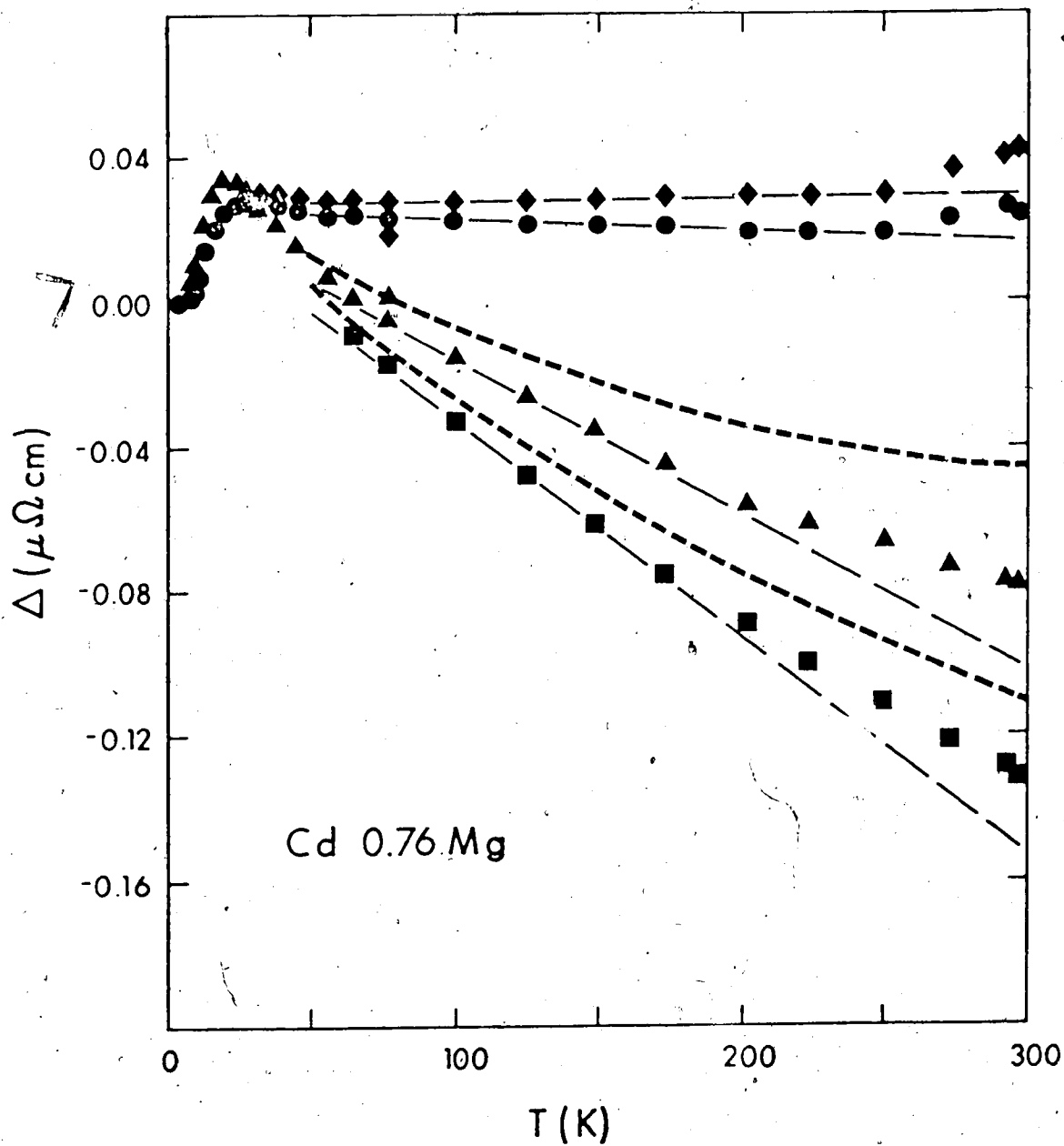
Fig. 9. Deviations from Matthiessen's rule Δ versus
temperature T for Cd0.76Mg of orientations:
●- $\theta = 89\frac{1}{2}°$, ◆- $\theta = 83\frac{1}{4}°$, ■- $\theta = 29°$ and
▲- $\theta = 16\frac{1}{2}°$. The bold dashed lines forming an
envelope on either side of the triangles represent
probable errors in absolute values of Δ.
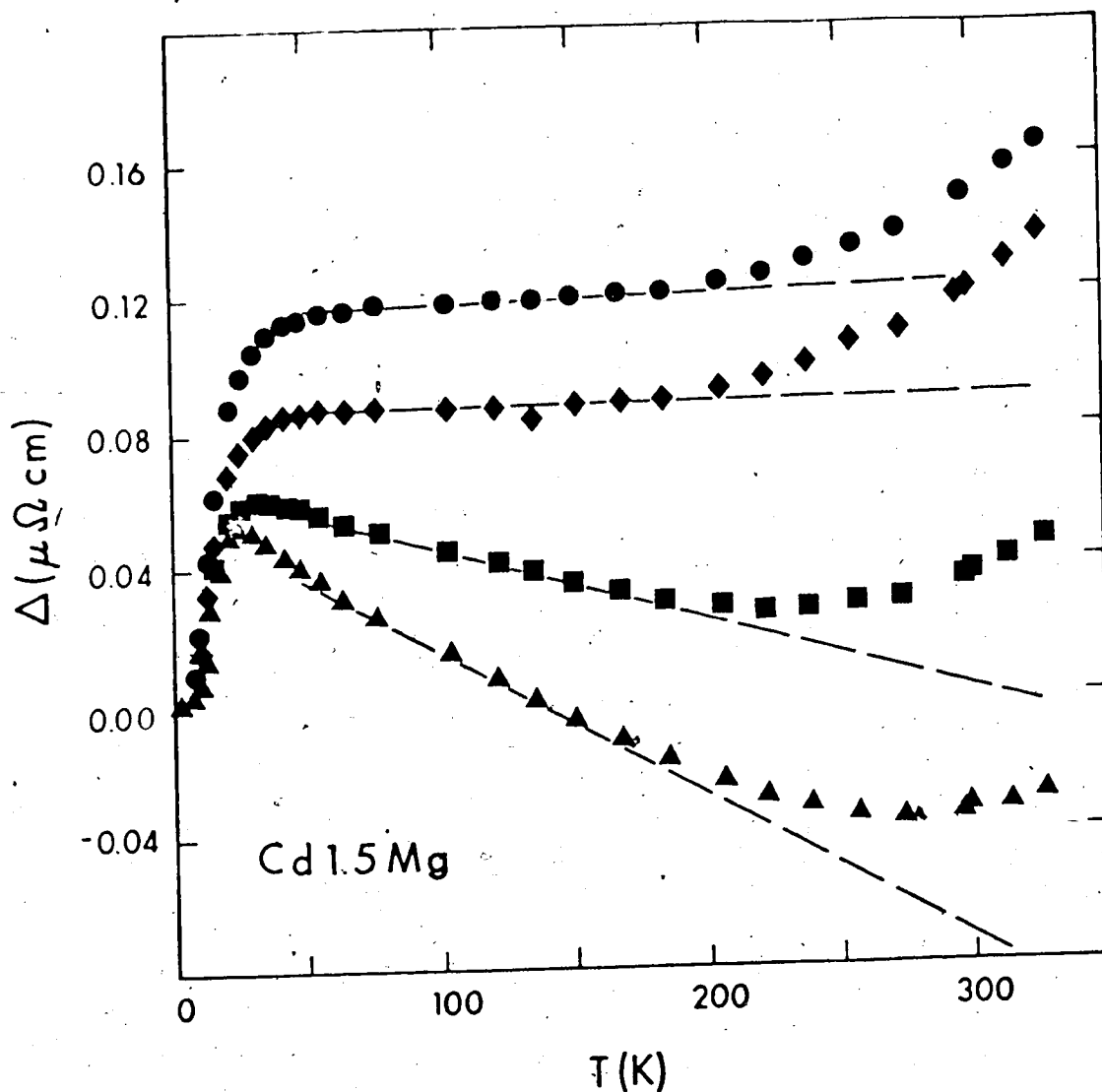
Fig. 10. Deviations from Matthiessen's rule Δ versus temperature T for Cd1.5Mg of orientations:
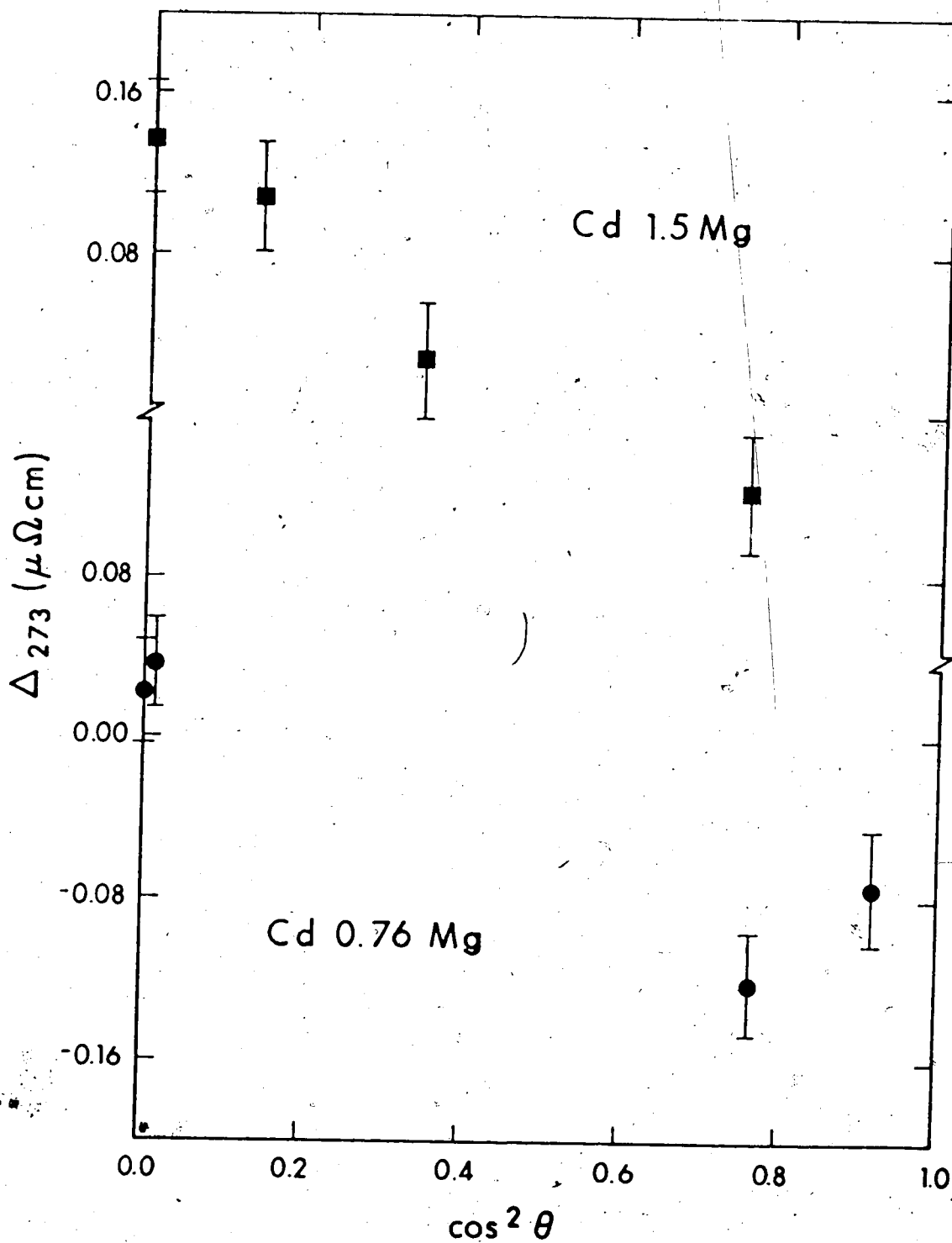●– θ = 87°, ◆– θ = 68°, ■– θ = 54° and ▲– θ = 29½°.

Fig. 11. Deviations from Matthiessen's rule at 273 K
(Δ_{273}) versus $\cos^2\theta$ for Cd0.76Mg (●) and
Cd1.5Mg (■).

found by Seth (1969) of $n \sim 5$ for Δ of polycrystalline specimens.

The ideal resistivities of pure Cd were also found to have power law dependence in the same temperature range, $\rho_i \propto T^n$ where $n = 5.7(\pm 0.2)$ for $\rho_{i||}$ and $n = 5.0(\pm 0.2)$ for $\rho_{i\perp}$. These values are consistent with those of 5.9 and 5.0 found by Alderson and Hurd (1975), although Alexandrov and D'Yakov (1963) find $\rho_i \propto T^5$ for both crystal orientations. Seth (1969) reports an exponent $n = 4.8$ for polycrystalline pure Cd specimens.

At somewhat higher temperature $T \sim 25$ K there is a hump in Δ (Figs. 9 and 10). The hump occurs where $\rho_{iT} \sim \rho_{Ao}$ and is more pronounced for the dilute alloys. Neither the hump nor the power law dependence is unusual and both have been discussed briefly from a theoretical point of view in Sec. 2.2. These, however, are not the features of central interest in this thesis.

At high temperatures, Δ is expected to be linear in T and may be either positive or negative (Bhatia and Gupta, 1969). Figs. 9 and 10 do show a linear region from about 75 K to 200 K but at higher temperatures yet, the slopes of the Δ-T curves increase to more positive values. Damon and Klemens (1965) predicted this type of feature would arise as a result of local phonon modes in binary alloys where the solute atoms are much lighter than the solvent atoms. They searched for this effect themselves

in gold alloys but failed to see it. Seth and Woods
(1970) show a similar increase in slope of their Δ-T curves
at about 200 K for $\underline{Cd}$-Mg polycrystalline specimens.
Because of their concern for possible preferred orienta-
tions, however, they did not interpret this behaviour
as arising from local modes.

The increase in slope should occur at $\sim \theta_0/2$ where
$\theta_0 = (M_i/M_o)^{1/2} \theta_D$ (see also Eqs. 2.10 and 2.11). For Cd,
$\theta_D \simeq 170$ K, so $\theta_0 \simeq 365$ K and the increase in slope due
to a local mode would be expected at about 180 K. Indeed,
this agrees roughly with our experimental results.

Local mode frequencies (and hence θ_0's) parallel
and perpendicular to the c axis should be proportional to
the square roots of the atomic force constants which are
quite anisotropic in Cd. Because the elastic constants
C_{33} and C_{11} are proportional to the atomic force constants[*],
local mode characteristic temperatures θ_0 should be roughly
proportional to the square roots of the elastic constants
as well. Indeed, the ratios $\theta_{0||}/\theta_{0\perp}$ (= 175/250 = 0.70
from Fig. 9 - this effect is not as pronounced in Fig. 10)

---

[*]The elastic constants, also depend on the lattice para-
meters, a and c. In a tetragonal lattice, for example,
$C_{11} = k_\perp/c$ and $C_{33} = k_{||}c/a^2$ where $k_\perp$ and $k_{||}$ are the
atomic force constants and we assume only nearest neighbour
interactions. Because the c/a ratio for Cd (1.889 at 293 K)
is only 14% greater than the close-packed value (1.633)
the anisotropy of the elastic constants C_{11}/C_{33} = 2.35 must
arise primarily from the anisotropy in the atomic force
constants.

and $\sqrt{C_{33}}/\sqrt{C_{11}}$ (= $\sqrt{4.9(\pm0.2)}/\sqrt{11.5(\pm0.5)}$ = 0.65($\pm$0.03) from

Alexandrov and Ryzhova (1961) are relatively close. Thus,

the relevant force constant for the local mode resistivity

is in the direction of the applied electric field. This

is expected since the probability of scattering an electron

from state $\vec{k}$ to $\vec{k}'$, $P(\vec{k},\vec{k}') \propto |\vec{u}\cdot(\vec{k}-\vec{k}')|^2$ where $\vec{u}$ is the

ionic displacement (see Ziman, 1969, p. 173).

The magnitude of the increase in slope is roughly

proportional to Mg concentration in this work and in that

of Seth and Woods (1970). This too is expected. We make

a preliminary estimate of the local mode resistivity above

Θ_0 by multiplying the ideal resistivity ρ_i of the host by

the atomic fraction of light impurity atoms x:

$$\Delta_4 \sim x\rho_i \qquad\qquad (5.5)$$

Estimates of Δ_4 based on this formula are in rough agree-

ment with experiments.

Thus, electron scattering from a local mode can

account for the magnitude, the concentration dependence,

the temperature and the anisotropy in temperature of an

otherwise unexplained feature of the resistivity of Cd-Mg

alloys. Although Damon and Klemens (1965) failed to see

this effect in gold alloys, the ideal resistivity of gold

is much lower than cadmium's so that according to Eq. 5.5,

they were looking for a much smaller effect. Secondly,

for their alloys $\rho_{1T} = \rho_{Ao}$ at a temperature much higher and closer to $\theta_o/2$ where Δ_4 becomes significant. Under these conditions, Δ_4 could have been masked by other contributions to Δ discussed in Sec. 2.2 (e.g. the hump in Δ is often located at temperatures where $\rho_{1T} \sim \rho_{Ao}$). We suggest further experiments to search for this local mode effect in other alloy systems.

We emphasize that the temperature dependence of our Δ-T curves (Figs. 9 and 10) is largely independent of errors in ℓ/A. These errors do not significantly affect the shape of the Δ-T curves and in particular, they do not affect the slope change which we associate with local modes.

Looking again at Figs. 9, 10 and 11, we also see qualitative agreement of our data with both the theoretical calculations of Toussaint and Pecheur (1973) for single crystals and with the experimental Δ-T curves of Seth and Woods (1970) for polycrystalline Cd-Mg. Seth and Woods did not expect the high temperature slopes of their Δ-T curves to be negative (see Ch. 1) and suggested their specimens may have preferred orientations. Although it now appears that their specimens did have preferred orientations (see Secs. 5.1 and 5.2), both pure and alloy specimens appear to have roughly the same preferred orientation, somewhat closer to parallel than expected, and consequently their Δ-T curves are roughly valid for that preferred orientation. Indeed, the similar shapes and magnitudes

of their curves to Figs. 9 and 10 confirms this interpretation.

In the meantime, Toussaint and Pecheur calculated Δ_3 in Cd-Mg single crystals which were negative at high temperatures, thus partially explaining Seth and Woods' results, and were an order of magnitude larger in the c direction than the a direction. Although they appear to have used pure metal pseudopotential matrix elements W_{Cd} and W_{Mg} in their calculations as opposed to pseudopotential matrix elements for the dilute alloy, the agreement of their theory with our experiments is remarkably good.

CHAPTER 6

CONCLUSIONS

We have measured the electrical resistivities from 2 K to 300 K for eight Cd single crystals and twelve Cd-Mg single crystals including three different concentrations. The measured densities of our specimens were typically 2½% below the accepted x-ray densities. This we attribute to small bubbles in the specimens and we have made an appropriate correction to obtain the resistivity values. The ice point resistivities for Cd were found to be $\rho_{||}$ = 7.81($\pm$0.03)$\mu\Omega$ cm and $\rho_{\perp}$ = 6.30($\pm$0.03)$\mu\Omega$ cm.

The resistivity anisotropy ratio $a = \rho_{||}/\rho_{\perp}$, for Cd as a function of temperature is in good qualitative agreement with the simple theory of Case and Gueths (1970) except at the lowest temperatures where a falls well below the predicted value of a_{∞} and where Case and Gueths' own work lacked the accuracy to test their low temperature prediction. That even a partial agreement exists is surprising, considering Case and Gueths' simplified model of the Fermi surface and their complete neglect of any effects due to anisotropy in the phonon spectrum. A better fit is to the calculated curve of White and Carbotte (1974) for Zn, perhaps a permissible comparison because of the similar c/a ratios and Fermi surfaces of Cd and Zn. The anisotropy ratios for the alloy specimens do not agree as well

as for the pure samples, but White and Carbotte have obtained isotropic residual resistivities in their calculations whereas experimental residual resistivities for Cd0.76Mg alloys are not isotropic.

Deviations from Matthiessen's rule were calculated for the Cd-Mg single crystals in the hope of clarifying the peculiar high temperature results in the Cd-Mg poly-crystals of Seth and Woods (1970). By comparing their polycrystal resistivities to ours for single crystals, we have shown that the polycrystals probably did have preferred orientations but the preferred orientations for both pure and alloy specimens were very similar. Their DMR are consequently comparable with our single crystal DMR. Our high temperature DMR are in good qualitative agreement with theoretical calculations by Toussaint and Pecheur (1973). In addition, the increase in slope of the Δ-T curves at about 200 K show all the salient but otherwise unexplained features for electron scattering from a local phonon mode. Although Damon and Klemens (1965) predicted and sought for this effect in gold alloys, it has not previously been recognized. In retrospect, Seth and Woods' results can also be explained in terms of Toussaint and Pecheur's calculations plus the effect of the local mode.

We emphasize that errors in the geometrical shape factors ℓ/A for our specimens and in the ~   for bubbles do not significantly affect the temperature

dependence of either k or DF. In particular, they do not affect our conclusions about the anisotropy ratio nor do they affect our conclusions about the local mode resistivity.

BIBLIOGRAPHY

Alderson J.E.A. and Hurd C.M. (1975), Phys. Rev. B 12, 501.

Alexandrov B.N. (1963) Sov. Phys. J.E.T.P. 16, 286.

Alexandrov B.N. and D'Yakov I.G. (1963) Sov. Phys. J.E.T.P. 16, 603.

Alexandrov B.N. and Ryzhova T.V. (1961) Sov. Phys. (Crystallography) 6, 228.

Alstad J.K., Colvin R.V. and Legvold S. (1961), Phys. Rev. 123, 418.

Bass J. (1972), Adv. Phys. 21, 431.

Bhatia A.B. and Gupta O.P. (1969), Phys. Letters 29A, 358.

Bridgman P.W. (1925), Proc. Am. Acad. Arts Sci. 60, 305.

Bridgman P.W. (1929), Proc. Am. Acad. Arts Sci. 63, 351.

Bridgman P.W. (1964), Collected Experimental Papers (Harvard), (papers 58 and 79 are the above two.)

Case S.K. and Gueths J.E. (1970), Phys. Rev. B 2, 3843.

Damon D.H. and Klemens P.G. (1965), Phys. Rev. 138, A1390.

Damon D.H., Mathur M.P. and Klemens P.G. (1968), Phys. Rev. 176, 876.

Das S.J. and Gerritsen A.N. (1964), Phys. Rev. 135, A1081.

Dugdale J.S. and Basinski Z.S. (1967), Phys. Rev. 157, 552.

Edwards, Wallace W.E. and Craig R.S. (1952), J. Am. Chem. Soc. 74, 5256.

Goens E. and Grüneisen E. (1932), Ann. Physik 14, 164.

Grüneisen E. (1945), Ergebn. exakt. Naturw. 21, 50.

Grüneisen E. and Goens E. (1923), Phys. ZS. 24, 506.

Grüneisen E. and Goens E. (1924), Z. Physik 26, 250.

Hansen M. (1958), Constitution of Binary Alloys (McGraw
Hill N.Y.).

Hedgcock F.T. and Muir W.B. (1964), Phys. Rev. 136, A561.

Hurd C.M. (1974), Adv. in Phys. 23, 315.

Kagan Y. and Zhernov A.P. (1966), Sov. Phys. J.E.T.P. 23,
737.

Kagan Y. and Zhernov A.P. (1971), Sov. Phys. J.E.T.P. 33,
990.

Klemens P.G. (1963), J. Phys. Soc. Japan Japan 18, Suppl
II, 77.

Koshino S. (1960), Prog. Theor. Phys. 24, 484, 1049.

Landauer R. (1952), J. App. Phys. 23, 779.

McCammon R.D. and White G.K. (1965), Phil. Mag. 11, 1125.

Meaden G.T. (1965), Electrical Resistance of Metals
(Plenum).

Mott N.F. and Jones H. (1958), The Theory of the Properties
of Metals and Alloys (Dover N.Y.).

Pearson W.B. (1958), A handbook of Lattice Spacings and
Structures of Metals and Alloys Vol. 1, (Pergamon).

Pecheur P. and Toussaint G. (1973), Phys. Stat. Sol. B 59,
K67.

Ridley N. (1964), J. Inst. Met. 93, 46.

Rowlands J.A., Stackhouse B.J. and Woods S.B. (1975),
Proc. 14th Int. Conf. Low Temp. Phys. (North-Holland,
Amsterdam), v.3, 110.

Seth R.S. (1967), M.Sc. Thesis, University of Alberta.

Seth R.S. (1969), Ph.D. Thesis, University of Alberta.

Seth R.S. and W ds S.B. (1970), Phys. Rev. B $\underline{2}$, 2961.

Sondheimer E.H. and Wilson A.H. (1947), Proc. R. Soc. A $\underline{190}$, 435.

Taylor P.L. (1962), Proc. Phys. Soc. $\underline{80}$, 755.

Taylor P.L. (1964), Phys. Rev. $\underline{135}$, A1333.

Toussaint G. and Pecheur P. (1973), Phys. Letters $\underline{45A}$, 75.

White B.A. and Carbotte J.P. (1974), J. Phys. F $\underline{4}$, 2223.

Ziman J.M. (1969), Principles of the Theory of Solids (Cambridge).

APPENDIX 1

NOTATION

Below is a list of frequently used symbols and definitions in this thesis:

θ (lower case theta) - specimen orientation, the angle between c axis and the specimen axis.

θ_T - denotes explicitly the dependence of orientation on temperature, T.

θ_O - orientation as $T \to 0$ K

θ_{293} - orientation at $T = 293$ K

Θ (upper case theta) - characteristic temperature

Θ_D - Debye temperature

Θ_O - Local mode characteristic temperature

$\Theta_{||}$ - Characteristic temperature for vibrations parallel to the c axis.

$\Theta_{\perp}$ - Characteristic temperature for vibrations perpendicular to the c axis.

ω - frequency, or characteristic frequency, appears with the same subscripts as Θ above.

ρ - electrical resistivity

$\rho(\theta)$ - denotes explicitly the dependence on orientation. Up to three subscripts are also used to denote explicitly the dependence on composition (ρ_i, ρ_A), axial orientations ($\rho_{||}$, $\rho_{\perp}$) and temperature (ρ_T, ρ_O, ρ_{273}) in that order. Up to three subscripts may be included in a single symbol (e.g. $\rho_{i||T}$).

(ρ_{ij}) - the resistivity tensor

ρ_i (often appearing as ρ_{iT}) the "ideal" resistivity of a high purity metal after its small residual resistivity has been subtracted.

ρ_P - the total resistivity of a "pure" metal specimen including the residual resistivity, therefore $\rho_{iT} = \rho_{PT} - \rho_{Po}$.

ρ_A - the total resistivity of an alloy specimen including the residual resistivity.

ρ_T - denotes explicitly the dependence of resistivity on temperature

ρ_{273} - resistivity at T = 273 K.

ρ_o - extrapolated residual resistivity at T = 0 K

ρ_{poly} - resistivity of a polycrystalline specimen.

$\rho_{||} = \rho(0°)$ - resistivity parallel to the c axis.

$\rho_{\perp} = \rho(90°)$ - resistivity perpendicular to the c axis.

ρ_{meas} - the measured value of resistivity

ρ_m - the resistivity of a mixture

We denote similarly in σ, Δ, a, R, f = ℓ/A and L the dependence on composition, orientation, and/or temperature.

σ - electrical conductivity

Δ - the total "deviation from Matthiessen's rule" (DMR) for an alloy specimen

Δ_3 - the contribution to Δ due to the interference term

Δ_4 - the contribution to Δ due to localized phonon modes

$a = \rho_{||}/\rho_{\perp}$ - anisotropy ratio

a_{∞} - the extrapolated value of a as $T \to \infty$.

a_{max} - the maximum value of a.

R - electrical resistance

R_s - resistance of a standard resistor.

Cd0.76Mg #5 - specimen number 5 made from the master alloy

of host Cd with 0.76 atomic percent Mg.

Cd-Mg - a dilute binary alloy of host Cd with

impurity Mg.

Cd-Mg - a binary alloy of Cd and Mg.

x - concentration, the atomic fraction of solute metal in

a binary alloy (in eq. 2.8 only, c is used for

concentration).

B - "Bubble factor", the fraction of the total specimen

volume occupied by bubbles or voids.

- B also denotes one of the constituents in a

binary (A-B) alloy.

c - c direction or c axis - the crystal direction (axis)

perpendicular to the hexagonal planes of six-fold

symmetry.

c - the lattice parameter in the c direction.

a - a direction or a axis - a crystal direction from an

atom towards a nearest neighbour atom in the same

hexagonal plane.

a - the lattice parameter in the a direction.

$f = f_{\vec{k}}$ - electron distribution function (appears in

Chapter 2 only).

$f = \ell/A$ - geometrical shape factor for specimens (appears in Chapters 3 and 4)

ℓ - the length between potential contacts on a specimen

ℓ' - the length of a specimen after it is cut for weighing ($\ell' \simeq \ell$).

L - appears in the form (L_T/L_{293}) which represents the fractional thermal contraction (or expansion), usually in a given direction. The subscripts $||$, $\perp$, and θ denote orientation.

A - usually in the form (ℓ/A), is the average cross-sectional area of a specimen.

    -as a subscript e.g. ρ_{AT} denotes an alloy specimen.

    -$A_{||}$ and $A_{\perp}$ in Chapter 2 only denote areas on the Fermi surface.

    - also denotes one of the constituents in a binary (A-B) alloy.

M_i and M_o - masses of the host and impurity atoms respectively in a dilute binary alloy.

$\vec{E}$ - electric field. E_i $i = 1,2,3$ are components of $\vec{E}$

$\vec{J}$ - electric current density. J_i $i = 1,2,3$ are components of $\vec{J}$

ϕ ...le between electric field $\vec{E}$ and current density $\vec{J}$ anisotropic crystals.

    ...ppears in Appendix 2 only.

$\vec{k}$ - ele... n wave number

k - $(k_{||},$ - ...arest neighbour atomic force constants

C_{11} (C_{33}) – elastic stiffness constants.

Other less frequently used symbols are defined in the text.

APPENDIX 2

TRANSVERSE ELECTRIC FIELD IN ANISOTROPIC METALS

In the long thin specimens used for resistivity measurements, the electric current density $\vec{J}$ is uniform and parallel to the specimen axis except near the current contacts. Even in metals with the simplest anisotropic crystal structures (hexagonal, tetragonal, and trigonal), the electric field, $\vec{E}$, is parallel to $\vec{J}$ only for specimens with parallel ($\theta = 0°$) or perpendicular ($\theta = 90°$) orientations. In general, for a specimen of orientation θ, the components of $\vec{E}$ can be found using:

$$
\begin{pmatrix} E_1 \\ E_2 \\ E_3 \end{pmatrix} = \begin{pmatrix} \rho_\perp & 0 & 0 \\ 0 & \rho_\perp & 0 \\ 0 & 0 & \rho_{||} \end{pmatrix} \begin{pmatrix} J\sin\theta \\ 0 \\ J\cos\theta \end{pmatrix}
\qquad \text{(A2.1)}
$$

The angle ϕ between $\vec{J}$ and $\vec{E}$ is

$$
\phi = \theta - \tan^{-1} [(\rho_\perp/\rho_{||})\tan\theta] \qquad \text{(A2.2)}
$$

$$
= \theta - \tan^{-1} [(\tan\theta)/a]
$$

For a cadmium single crystal ($\rho_{||}/\rho_\perp = 1.237$ at 295K) of orientation $\theta = 45°$, $\phi = 6.05°$. The transverse component of $\vec{E}$ is not negligible and could be measured.

For a given orientation and current density, the transverse electric field ($\vec{E}\sin\phi$) depends only on the anisotropy ratio $a = \rho_{||}/\rho_{\perp}$ and is approximately proportional to $(a-1)$. Tables relating ϕ and a are easily constructed. The transverse electric field is thus a measure of the anisotropy ratio. Since an average resistivity

$$\rho(\theta) = \left[\rho_{||}\cos^2\theta + \rho_{\perp}\sin^2\theta\right] \qquad (A2.3)$$

can be measured in the conventional method using the longitudinal field ($E\cos\phi$), both $\rho_{||}$ and $p_{\perp}$ can be found by two measurements on the same specimen.

The specimen geometry suggested for this type of measurement is a rectangular prism with $\ell \gg w \gg h$, typically 20 cm x 1 cm x 0.2 cm, and with the c-axis lying in the ℓw plane. Such specimens could either be cut from larger crystals or grown from seeds in molds of the desired shape. In order that the transverse potential contacts do not sample a small part of the longitudinal potential difference, it will be important that these contacts are located accurately opposite each other. An uncertainty of ± 0.02 cm would produce an uncertainty in a of $\pm 19\%$ for a cadmium crystal of orientation 45° and the above typical geometry. Unlike Hall effect measurements where the external magnetic field can be turned off while the

unwanted longitudinal potential is adjusted to zero,

there is no way of "turning off" the transverse field

without turning the longitudinal field off too.   A

specimen holder could, however, be checked or calibrated

using an isotropic metal. This method of resistivity

measurement does offer some advantages, particularly for

anisotropic alloy crystals where concentrations may vary

among specimens.

APPENDIX 3

SUGGESTIONS FOR FUTURE RESISTIVITY MEASUREMENTS

The largest errors in this work are in the measurements of $(\ell/A)_{295}$ which are the culmination of many small errors. Even though the improvement in accuracy due to the suggestions below may seem almost trivial, maximum precision at all stages is vital in obtaining Δ with reasonable accuracy.

(1) Specimen diameters should be tripled to about 3 mm. Size effects at the lowest temperatures would be less important, the accuracies of the cross-sectional areas determined by weighing and by micrometer measurements would be increased and specimens would be both easier to handle and stronger. Although sharper x-ray diffraction patterns for thick specimens are probably due in part to the smaller radius of curvature, I suspect there is also less strain in thick specimens. Whatever the cause, the accuracy of the orientation determinations could be increased somewhat. Although the resistance and thus the IR drop is inversely proportional to cross-sectional area our voltage sensitivity has increased by an order of magnitude with the acquisition of the current comparator since Seth and Woods' (1970) work so that we can afford to lose an order of magnitude in the value of R. In fact, the current could also be tripled without increasing the

heat dissipation I^2R in the specimens themselves, beyond that presently dissipated, and consequently, the loss in voltage IR would only be a factor of three.

.(2) Specimens should continue to be mounted in a holder which allows free expansion as well as contraction and the current connections should continue to be soldered to the specimens. Potential contacts, however, should be redesigned to be spring-loaded, such as the knife-edge contacts shown by Case and Geuths (1970). These would ensure electrical contact throughout the run and would hopefully avoid the small resistance changes we occasionally observed due to thermal cycling. Knife-edges transverse to the specimen length are probably preferable to point contacts as the indentations they make in the specimen are likely to produce smaller uncertainties in ℓ.

(3) Alloy specimens should be dilute with impurity concentrations of about 1 atomic percent or less. This should both reduce uncertainties in densities (which in Cd-Mg, for example, is fairly strongly dependent on concentration which, in turn, is difficult to determine with great precision) and minimize the possibility of atomic ordering in the lattice.

(4) Specimens should be cut prior to weighing with a spark-cutter, for example, to maximize the accuracy of ℓ'.

.(5) Densities of all specimens should continue to to be measured and compared to x-ray values to determine

the size of the bubble factor, if any. Efforts should be made to reduce or eliminate bubbles. In spite of rapid evaporation, it would probably be worth trying Bridgman's (1925) technique of washing molten metals back and forth under a vacuum to get rid of occluded gas. Although the mold material may not play a role in this process, bubble factors should be compared for specimens grown in glass and graphite molds. It is also possible that graphite molds produce less strain in the specimen. Alderson and Hurd (1975) measured 3 mm diameter specimens grown in graphite molds up to 587 K with only a small change in resistivities on returning to room temperature. Alexandrov (1963) also used graphite molds for Cd even though glass molds and hydrofluoric acid were used for other metals (In, Pb, Bi) in the same study. If glass molds and HF are used, the acid should not be used until excessive amounts of time are required to dissolve the glass and the specimens should be rinsed thoroughly after the HF 'etch'. In preliminary runs, some specimens show an unusual decrease in resistivity below about 4 K which we attribute to a black residue left on some specimens after the HF etch.

APPENDIX 4

CHANGE OF SINGLE CRYSTAL ORIENTATION DUE TO ANISOTROPIC

THERMAL CONTRACTION

In Figure 12(a) it can be seen that:

$$\tan \theta_{293} = n_a a_{293}/n_c c_{293} \qquad (A4.1)$$

where θ_{293} is the angle between the specimen axis and the c axis at 293 K (i.e. the crystal orientation), a_{293} (c_{293}) is the length of the a (c) lattice parameters at 293 K, and n_a (n_c) is the number of a (c) lattice vectors going from one side of the crystal to the other in a direction parallel to the a (c) axis.

Similarly, in Figure 12(b)

$$\tan \theta_T = n_a a_T/n_c c_T \qquad (A4.2)$$

where θ_T, a_T, and c_T are the crystal orientation and lattice parameters at temperature T. Eliminating n_a/n_c from Eqs. A4.1 and A4.2

$$\tan \theta_T = (c_{293}/a_{293})(\tan\theta_{293})(a_T/c_T)$$

$$= \frac{(a_T/a_{293})}{(c_T/c_{293})} \tan \theta_{293} \qquad (A4.3)$$

$$= \frac{(L_T/L_{293})_\perp}{(L_T/L_{293})_{||}} \tan \theta_{293} \; .$$

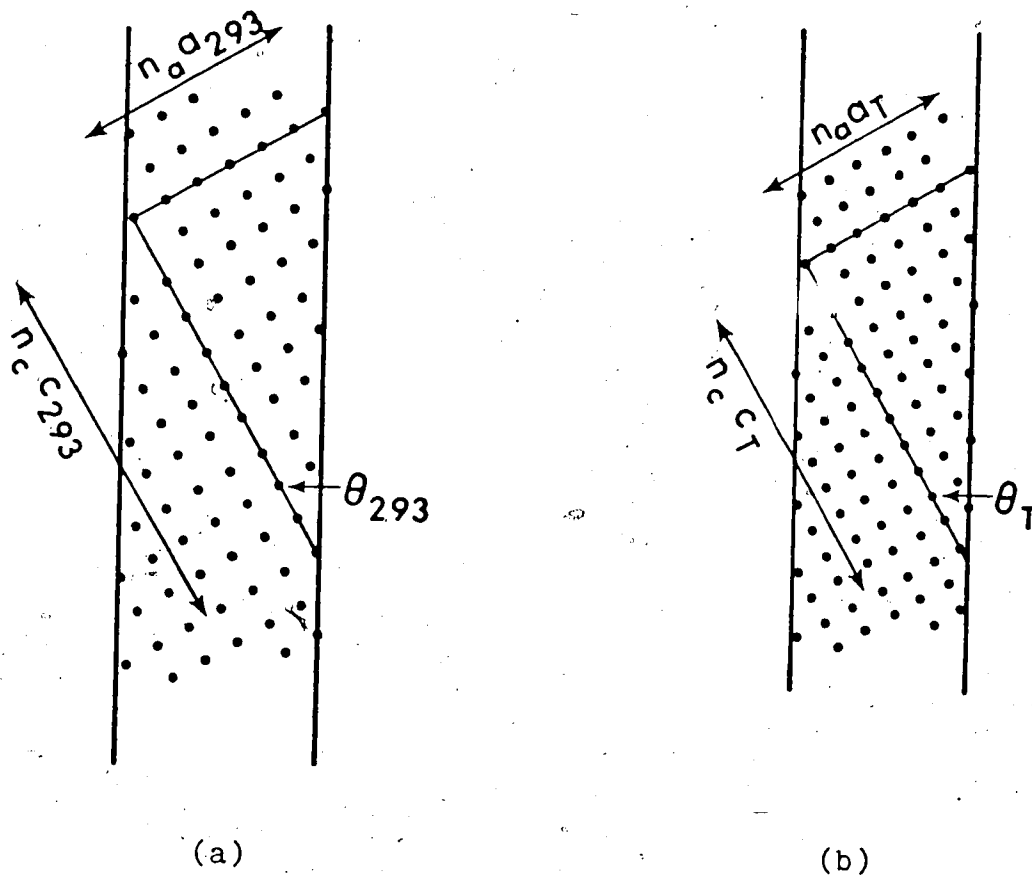(a)   (b)

Fig. 12.   Change of orientation due to anisotropic thermal
           contraction. The above diagrams represent a
           single crystal showing atomic s. es at (a) 293 K
           and (b) T < 293 K where there has been a decrease
           in c of 20% and a decrease in a of 10%.

Values of $(L_T/L_{293})_{||}$ and $(L_T/L_{293})_\perp$ are given in Table 3 so that θ_T can be calculated knowing T and θ_{293}.